PCCP

ROYAL SOCIETY OF CHEMISTRY

PAPER

View Article Online
View Journal | View Issue

Cite this: *Phys. Chem. Chem. Phys.*, 2026, **28**, 2111

Single-atom Pd in ZSM-5 for selective oxidation of methane to methanol: a DFT-based ONIOM approach

Priyanka Dutta,[a] Nishant Biswakarma,[a] Dikshita Dowerah,[ab] Shilpa Neog,[a] Nand Kishor Gour,[a] Gaurisankar Phukan[a] and Ramesh Chandra Deka *[ac]

Single-atom catalysts are emerging as promising candidates for the selective oxidation of methane, providing distinctive opportunities to improve activity, selectivity, and atomic efficiency. In this study, we have applied the DFT-D3 based ONIOM approach to examine the potential energy surfaces of Pd single atoms, with oxidation states of 0, +1, and +2, enclosed within the ZSM-5 framework for the partial oxidation of methane to methanol employing N_2O as the oxidant. We have incorporated dispersion correction using Grimme's GD3 dispersion correction to account for the van der Waals interaction within the zeolite's framework. The isomorphous substitution of the framework Si atoms with the Al atoms caused the zeolites to have negative charges, which are balanced by metal cations or protons. Depending on the oxidation states of the Pd atom, we have substituted Si atoms with an equivalent number of Al atoms to maintain the overall charge neutrality of the ZSM-5 framework. The mechanism of the reaction mainly consists of three key steps: formation of the active site by N_2O, activation of the C–H bond of methane and recombination of the CH_3 and OH moieties to form methanol. Two-state reactivity has also been considered for the catalyst with close lying spin states. Furthermore, the inclusion of water during methanol desorption significantly reduces its desorption energy, thereby preventing the risk of over-oxidation and increasing the selectivity. In terms of activation barrier, kinetic analysis and methanol desorption energies, siliceous ZSM-5 with Pd^0 is found to be the most favorable choice for partial oxidation of methane to methanol. Our findings offer significant insights into the oxidation state dependent reactivity of single atom Pd/ZSM-5 for direct conversion of methane to methanol.

Received 4th August 2025,
Accepted 9th December 2025

DOI: 10.1039/d5cp02968f

rsc.li/pccp

Introduction

Climate change constitutes an important worldwide issue facing mankind in the 21st century.[1] Greenhouse gases profoundly affect the global ecosystems and biodiversity by disrupting natural processes and intensifying environmental instability.[2] While CO_2 is the most predominant greenhouse gas, methane possesses a substantially greater global warming potential, rendering it the second most critical contributor to atmospheric warming.[3] Consequently, it is necessary to reduce methane emissions from natural gas engines and other heating sources. A method for mitigating methane is the advancement of effective technologies for its valorization, which is also a century long process. Additionally, methane is the main constituent of natural gas, which possesses potential utility as a cleaner source of fossil energy and as a raw material, contingent upon its inexpensive transportation to the place of application. In this regard, converting methane on-site and on a large scale into transportable high-dense fuels or high value-added compounds, like liquid oxygenates, aromatics, and hydrogen, would be highly beneficial.[4] Nonetheless, the on-site conversion of methane is challenging due to its chemical inertness.[5] Thus, conversion of methane into value-added products is crucial, as it not only addresses the urgent need to mitigate methane emissions but also transforms this potent greenhouse gas into cleaner energy sources and valuable raw materials, thereby playing a significant role in combating climate change.

Originally, the manipulation of methane was considered as the "clavis aurea", an intractable yet rewarding challenge, making it the focus of extensive investigation. Direct conversion of methane to methanol has garnered significant attention due to the high hydrogen content, low carbon emissions, and versatility of methanol as a clean fuel and chemical feedstock.[6–9] Direct

[a] *CMML-Catalysis and Molecular Modelling Laboratory, Department of Chemical Sciences, Tezpur University, Napaam-784028, Assam, India. E-mail: ramesh@tezu.ernet.in*
[b] *Department of Chemistry, Arunachal University of Studies, Namsai-792103, Arunachal Pradesh, India*
[c] *Department of Chemistry, Cotton University, Panbazar, Guwahati-781001, Assam, India*

oxidation of methane to methanol continues to pose a significant challenge in catalysis and industrial chemistry because of the inherent stability of the C–H bond in the methane molecule and the relatively high reactivity of methanol.[10–12] The existing two-step process employed by industries for methane utilization is highly energy-intensive due to the elevated temperature and pressure requirements.[13] A most effective method for the utilization of CH_4 is the direct conversion of CH_4 to CH_3OH under mild conditions at relatively low temperatures, as this transformation is thermodynamically viable at such temperatures. However, the implementation of this method has proven difficult due to the absence of an appropriate catalyst.[14] The use of catalysts offers an optimal solution for reducing the high energy costs associated with these processes.[14] The naturally occurring copper-containing enzyme methane monooxygenase[15] can activate methane at room temperature; however, industrial-scale operation remains unfeasible. Thus, a significant amount of research has been dedicated to enhancing the catalytic capabilities of existing catalysts such as transition metal oxides,[16] clusters,[17,18] metal–organic frameworks,[19,20] zeolites[21,22] *etc.*, indicating the need to create a new class of catalytic materials.[23,24]

Single atom catalysts (SACs) have emerged as a new class of catalysts and have attracted growing interest in the field of catalysis.[23,25] Different from those of bulk metal clusters or nanoparticles, SACs have extraordinary chemistry, which provides selectivity, activity and stability.[25] Due to their optimal atomic efficiency and well-defined catalytic centers, single-atom catalysts (SACs) have emerged as both extremely effective catalysts and exemplary models for exploring the structure–performance connection.[26] The catalytic effectiveness of SACs has been observed in various processes like CO oxidation, CO_2 hydrogenation, O_2 reduction reactions, *etc.*[27] SACs with precisely coordinated metal centers on active supports have exhibited remarkable reactivity and selectivity for methane oxidation, owing to their ability to facilitate the reaction under mild circumstances.[28] Supports play a key role in stabilizing SACs. Diverse supports, including metal oxides, metals, two-dimensional (2D) materials, zeolites, and metal–organic frameworks, have been utilized to stabilize single atoms by anchoring them on surfaces or integrating them into frameworks.[29,30] Sun *et al.*[31] carried out a mechanistic investigation of conversion of methane to methanol on single atom 3d transition metal modified graphyne using molecular O_2 as an oxidant. Dispersed single metal atoms on graphyne supports have been discovered to replicate the enzymatic production of catalytically active M–O moieties, which are crucial for the kinetics of methane oxidation. A detailed mechanistic study was carried out using a single Rh atom dispersed on ZrO_2 for the oxidation of methane to methanol, where it has been observed that the oxide support prevents the over oxidation to CO_2.[32]

Among all support systems, zeolite supports are attractive due to their exceptional stability, homogeneous pore structure, and low synthesis cost.[30–35] Within this group of catalysts, ZSM-5 is of particular interest owing to its unique MFI structure, which gives it the best combination of microporosity and accessibility for catalytic use.[33] It is even more suitable as a support system because of its simple synthesis and resistance to the extreme reaction conditions.[34,35] ZSM-5 has a unique channel structure, tunable acidity and shape selective properties. These features help to stabilize metal centers within the framework and facilitate the transformation of small molecules like CH_4, CO_2, *etc.* into value added products.[36–38] In a combined theoretical and experimental study, Guo *et al.*[39] used the single atom catalyst Cu_1/ZSM-5 for the selective oxidation of methane to oxygenates. They revealed that each isolated Cu atom, stabilized by four O moieties on the ZSM-5 support, contains a uniform Cu_1–O_4 entity as an active site and preferentially activates CH_4 over CH_3OH, which is useful for the highly selective synthesis of C1 oxygenates, particularly methanol. An Rh single atom catalyst supported on hydrophobic ZSM-5 with CO and O_2 was reported to oxidize methane to C1 and C2 oxygenates under relatively low pressure.[40] Hu *et al.*[41] also used Rh@ZSM-5 as a model catalyst for the methane partial oxidation, where they investigated the effect of CO and H_2O on the overall energetics of the reaction. Pd-encapsulated ZSM-5 was employed in the investigation of alkyne semi-hydrogenation, which was shown to be extremely efficient.[42] Thus, the zeolites' unique properties make them invaluable for advancing catalytic processes and optimizing methane conversion to valuable products.

Noble metal catalysts (Pt, Pd, and Rh) have shown excellent performance towards the methane oxidation reaction.[43,44] Palladium or palladium based catalysts and their oxides have significantly greater reactivity for methane oxidation compared to other transition or noble metal catalysts.[44–47] Epling and Hoflund[48] investigated catalytic methane oxidation using ZrO_2-supported Pd catalysts and discovered that augmenting the Pd loading from 0.1 to 10 wt% enhanced catalytic performance. Guo *et al.*[49] conducted a catalyst synthesis method to manipulate the local environment of highly scattered metal-active sites through the targeted deposition of Pd next to highly dispersed ZrO_x on the ZSM-5 zeolite, utilizing electrostatic interactions for methane oxidation. Li *et al.*[50] demonstrated the catalytic efficiency of Pd@Na-ZSM-5 for methane oxidation at varying Si/Al ratios, with Si/Al = 40 exhibiting the maximum catalytic activity. Fan *et al.*[51] observed that in Pd@ZSM-5, the acidity of zeolite influences lean methane oxidation, with a reduction in acid sites enhancing catalytic performance. The microporous MFI channels of ZSM-5 effectively confine Pd atoms in the dispersed state, which avoids agglomeration and maximizes metal utilization. Such arrangements additionally promote the formation of well-defined active sites that contribute to the selective activation of species.[51,52] Wang *et al.*[53] reported that the acidic nature of supports significantly impacted the performance of supported Pd catalysts for catalytic combustion of methane. PdO dispersion depended on acid sites, with Lewis acid sites being more decisive for dispersing and stabilizing PdO_x. Also, it was found that the existence of Lewis acid sites was essential for the dispersion and stabilization of PdO. Petrov and his coworkers presented an innovative method for synthesizing a sintering-resistant Pd/zeolite catalyst and validated its efficacy in the challenging methane oxidation reaction.[54] Thus, Pd based catalysts have shown promising activity towards the methane oxidation

reaction, which can be further tuned by selecting appropriate support systems.

In this work we have used a Pd@ZSM-5 single atom catalyst for the partial oxidation of methane to methanol using N_2O as an oxidant.[55,56] N_2O ranks as the third most prevalent greenhouse gas, following CO_2 and CH_4. The increasing concentrations of N_2O in the atmosphere have garnered significant attention due to its involvement in several detrimental chemical reactions, including those that contribute to the formation of photochemical smog and acid rain. Consequently, it can function as an oxygen transfer agent, releasing environmentally friendly N_2 into the atmosphere.[57] The complete pathway has been demonstrated using 3 different oxidation states of Pd, mainly Pd^0, Pd^{1+} and Pd^{2+}. The reactivity of siliceous zeolites *vs.* aluminosilicate zeolites towards methane activation has been observed. A comparative analysis of the first and second C–H activation steps was performed to determine the catalyst best suited for promoting selective formation of the desired product. These results are expected to contribute to a deeper understanding of catalytic mechanisms and may guide subsequent research efforts in this direction.

Computational details

The partial oxidation of methane to methanol on Pd^n@ZSM-5 (n = 0, +1, +2) has been investigated by a DFT based hybrid QM/MM (quantum mechanics/molecular mechanics) electronic embedded two layer ONIOM (Our-Own-Layer-Integrated-molecular orbital) approach.[58–60] Hybrid QM/MM methodologies are proficient in investigating the catalytic properties of active sites in nanometer-scale zeolites.[61] They integrate precise quantum mechanical approaches such as density functional theory (DFT) to monitor reactions at the active site quantum mechanical region (QM, internal region) with less computationally intensive molecular mechanics (MM) methods to simulate the surrounding zeolite structure (external environment). The ONIOM method offers distinctive advantages over conventional additive QM/MM methods. ONIOM is a prevalent partitioning approach effectively validated in the numerous condensed phase systems, including both solution and heterogenous catalysis. In particular, ONIOM has also proven to efficiently describe the structure of the environment as well as capture the mid- and long-range polarization and electrostatic effects on the active site.[62] Farhan and Sajith in a recent study showed the successful application of zeolite supported systems, including metal exchanged frameworks, confirming their reliability for catalytic studies.[63] In contrast to the traditional QM/MM methodologies, ONIOM does not explicitly calculate the QM/MM interaction Hamiltonian, which significantly enhances the computational efficiency. Furthermore, its integration into the Gaussian has an automatic link atom treatment that adjusts the boundary bonds to maintain a continuous potential energy surface facilitating stable geometry optimization and molecular dynamics. In addition, owing to the interactions of the link atom host with the model system at a low theoretical level, it partly compensates the error generated by the use of link atoms.[60]

The predominant method for modeling zeolites involves a cluster approach.[64,65] ZSM-5 used in our study is represented by the cluster model of formula $H_{74}O_{219}Si_{128}$, where H atoms are used to saturate the terminal oxygen atoms.[66] The QM region is constructed, compromising the T12 site containing a 10 membered sinusoidal ring ($Si_{10}O_{10}$) along with two additional Si and O atoms (Si_2O_2), and the rest of the regions are treated with MM calculations. The visual representation of the ZSM-5 cluster along with the layer division is shown in Fig. S1. To encapsulate the Pd^0, Pd^{1+} and Pd^{2+} transition metal atoms, the Si atom in the T12 site is replaced with 0, 1 and 2 Al atoms respectively. The placement of the Al atom is done following the Lowenstein rule.[67,68] To perform the DFT calculation in the QM region of the two-layer model, we have implemented the hybrid B3PW91 (Becke 3 parameter Perdew Wang 91) functional,[69] in conjunction with the LANL2DZ[70] basis set for the Pd atom and the 6-31G(d,p)[71] basis set for the H, C, O, Si, and Al atoms. To validate the method and level of theory used in the calculations, we have studied the multireference character (Tables S1–S3) and benchmarked with 10 different functionals (Table S4). Accurate modeling of adsorption and catalytic processes in zeolites requires the inclusion of dispersion corrections, as these govern the long-range interactions crucial for the framework–guest stabilization and understanding the underlying mechanism of the reaction mechanisms. The Grimme-D3 dispersion correction[72] was integrated into our analysis to address the influence of van der Waals interactions on the structural and electrical characteristics of the species in the quantum mechanical domain. We utilized UFF[73] to describe the atoms treated with molecular mechanics, referred to as MM atoms, which has been used widely for the various catalytic reactions on zeolites due to its simplicity. UFF provides a reasonable or adequate representation of zeolites frameworks, yielding favorable geometries and non-bonded interactions for the silica/alumina structure.[63,74–78] All the atoms in the QM region along with atoms connecting QM and MM regions are fully relaxed. The existence of a single imaginary frequency in the vibrational spectra validates the transition phases, while no imaginary frequencies are detected for the reactants, intermediates, and products. Intrinsic reaction coordinate (IRC)[79] calculation has been conducted to assess the reliability of the reaction pathway. The free energy of activation ($\Delta G^{\neq}$) for the transition states is determined by assessing the free energy variation of the transition state relative to the initial state.

The adsorption of N_2O and CH_4 on Pd^n@ZSM-5 and PdO^n@ZSM-5 has been calculated using the following formula

$$E_{ads(N_2O)} = E_{N_2O\_Pd@ZSM\text{-}5} - E_{N_2O} - E_{Pd@ZSM\text{-}5} \quad (1)$$

$$E_{ads(CH_4)} = E_{CH_4\_PdO@ZSM\text{-}5} - E_{CH_4} - E_{PdO@ZSM\text{-}5} \quad (2)$$

where $E_{N_2O\_Pd@ZSM\text{-}5}$, E_{N_2O} and $E_{Pd@ZSM\text{-}5}$ are the zero-point corrected energies of N_2O adsorbed on Pd@ZSM-5, N_2O and Pd@ZSM-5 respectively. Similarly, $E_{CH_4\_PdO@ZSM\text{-}5}$, E_{CH_4} and $E_{PdO@ZSM\text{-}5}$ are the zero-point corrected energies of CH_4

adsorbed on PdO@ZSM-5, CH_4 and PdO@ZSM-5 respectively. The free energy of activation ($\Delta G^{\neq}$) for the transition states is determined by assessing the free energy variation of the transition state relative to the initial state. NBO analysis (Gaussian NBO 3.1) has been carried out to study their chemical behavior.[80] All the calculations have been carried out using the Gaussian 16[81] software package.

Kinetics study

The rate constant for each step in a catalytic oxidation reaction is derived using established kinetic theory, namely transition state theory (TST),[82] and is typically represented by the following equation:

$$k = \Gamma(T)\frac{k_B T}{h} e^{\frac{-\Delta G^{TS}}{RT}} \quad (3)$$

where $\Gamma(T)$ is the transmission coefficient, derived from the subsequent expression:

$$\Gamma(T) = 1 + \frac{1}{24}\left(\frac{h\upsilon\#}{k_B T}\right)^2 \quad (4)$$

In eqn (3), ΔG^{TS} represents the difference in Gibbs free energy between the transition state (TS) and the reactants. In eqn (4), $\upsilon\#$ denotes the magnitude of the imaginary frequency of the transition state (TS). Other terms maintain their conventional definitions.

Results and discussion

The schematic diagram for the partial oxidation of methane with N_2O in Pd^n@ZSM-5 (n = 0, 1, 2) is shown in Scheme 1. In the scheme, M stands for transition metals (Pd in our work), while N represents either Si or Al, depending on the formal oxidation state of the Pd atom. For the neutral Pd^0, N is Si, and for Pd^{1+} and Pd^{2+}, N is Al. The formal oxidation state of the Pd species is denoted by the superscript "n". The conversion reaction proceeds in 3 main steps. The steps are mainly (i) the formation of active M–O species reacting with N_2O and by releasing N_2,[63,83–85] (ii) activation of the 1st C–H bond of methane, and (iii) recombination of CH_3 and OH groups to form methanol and also to compare the activation barrier of 2nd C–H activation *vs.* CH_3 and OH groups to selectively oxidise methane to methanol instead of carbene and water. This article presents a comprehensive analysis of the partial oxidation of methane to methanol, beginning with the determination of the ground state configuration, followed by examination of the entire reaction pathway and comparison of the first and second C–H activation of methane.

We have considered the ground spin state configuration of Pd^n@ZSM-5 for the oxidation of methane to methanol with N_2O as the oxidant. First three spin states of each state of Pd^n@ZSM-5 has been considered and the reaction was carried out with the ground spin state in each case. The ground spin state is singlet for Pd@ZSM-5 and Pd^{2+}@ZSM-5, and doublet for Pd^{+}@ZSM-5. The results align well with the experimental ground states acquired by several techniques, including electron paramagnetic resonance (EPR) spectroscopy, for the Pd@ZSM-5 system.[86,87]

All the calculations including geometry optimization and transition state calculations were performed considering the ground state of Pd@ZSM-5 and Pd^{1+}@ZSM-5 as the energy difference between the ground state and the 1st excited state is very high. On the other hand, as the energy difference between ground and 1st excited states in Pd^{2+}@ZSM-5 is less than 9 kcal mol^{-1}, we have taken two-state reactivity into account for this particular zeolite system.

Partial methane oxidation to methanol using Pd@ZSM-5

Siliceous zeolites are frequently used as superior supports for Pd-based methane oxidation catalysts owing to their stability, anchoring capacity, and efficacy in diverse settings.[22,88,89] In this study we have used Pd@ZSM-5 in the ground singlet state to study the partial oxidation of methane using N_2O as the oxidant.

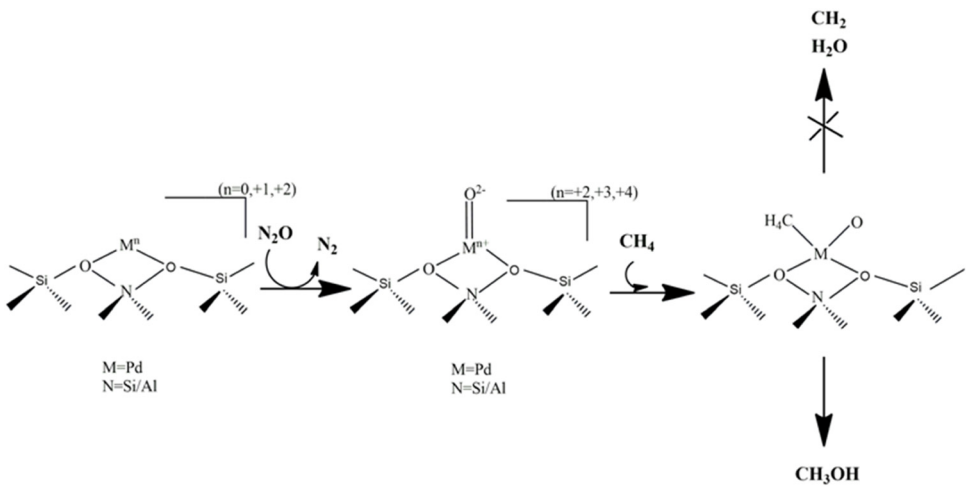

Scheme 1 Schematic representation of steps involved in the partial methane oxidation.

From the molecular orbital diagram (HOMO–LUMO diagram) shown in Fig. S2, it is observed that it is a closed shell configuration where the HOMO is delocalized over $4d_{z^2}$, $4d_{x^2-y^2}$, $4d_{xz}$ and $4d_{yz}$ orbitals, whereas the LUMO is mainly localized in the 5s orbital of Pd respectively. The electron density on the Pd atom indicates its axial donation capability, whereas the LUMO in the s orbital reflects the electrophilic nature, making it capable of accepting electrons. The orbital analysis indicates a stable yet reactive Pd center capable of catalytic reactions. The various positions of Pd atom encapsulation on the QM region of the ZSM-5 framework along with the adsorption energy are shown in Fig. S3. The optimized diagram involved in the reaction pathway is shown in Fig. 1, where after a specific intermediate the plausible formation of two products *via* two pathways is shown. The reaction proceeds with the adsorption of N_2O *via* the N-terminal on the Pd atom to form IM1 as shown in Fig. 1 as the adsorption energy *via* the N terminal side is more than that of the O-terminal side by 8.09 kcal mol^{-1}. We have presented the optimized diagrams of N-terminal and O-terminal N_2O adsorption on Pd@ZSM-5, along with the corresponding adsorption energy, in Fig. S4. As the reaction progresses after the initial N_2O adsorption as shown in Fig. 1, it proceeds towards N–O dissociation to form the active Pd–O species which will further involve in the methane oxidation process. The activation of the N–O bond occurs *via* TS1 ($-313.39i$), resulting in the formation of Pd–O (IM3), following the release of N_2, with a calculated bond length of 1.803 Å, which is close to the experimental value of 1.996 Å.[90] In IM3, the Pd atom possesses a positive atomic charge of $+0.264e$, whereas the charge on the O atom is $-0.550e$. From the NBO analysis, it has been found that the HOMO is localized on the $2p_y$-orbital of the O-atom and the $4d_{yz}$ orbital of the Pd atom, whereas the LUMO is localized on the $2p_z^*$ antibonding orbital of the O-atom as well as the $4d_{xz}$, $4d_{z^2}$ and 5s orbitals of the Pd atom. With the Pd–O bond defined as the *z*-axis, the LUMO offers axial σ* directionality, making the site electrophilic, and the π* component ($4d_{xz}$) enables the out of plane polarization. The axial polarization is also strengthened by the framework → metal donation. Methane is adsorbed on the active Pd–O species *via* the H atom of CH_4 with an endothermic adsorption energy of 1.62 kcal mol^{-1} in IM4. In IM4, the Pd adsorbed C–H bond and the C–H bond closer to the O atom slightly elongated compared to the rest of the two C–H bond lengths as shown in Fig. 1. The Pd adsorbed C–H bond elongated due to the formation of the Pd–H bond; however, this bond is not further activated due to the positive charge on both H and Pd atoms. In contrast, the C–H bond of methane next to active O species is activated through TS2, which has a single imaginary frequency of $-447.82i$ cm^{-1}, leading to complete dissociation into Pd–OH and Pd–CH_3 species (IM5). NBO analysis indicates a significant donor–acceptor interaction between the lone pair of the active O atom and the antibonding σ*(C–H) orbital ($E^{(2)}$ = 29.73 kcal mol^{-1}) that accounts for the polarization and weakening of the C–H bond. This interpretation along with the decrease in orbital occupancy in σ(C–H) (1.94 → 1.87) demonstrates that the methane activation proceeds *via* heterolytic C–H cleavage at the Pd–O site. From IM5, there are two possibilities for the reaction pathway. Pathway 1, which is also the desired one, is the recombination of CH_3 and OH moieties to form methanol and pathway 2 is activation of the 2nd C–H bond of methanol to form CH_2 and water. We have carried out both the pathways as shown in Fig. 1. Consequently, beginning with IM5, we have produced methanol (IM6) through TS3, where CH_3 and OH recombine. Starting from the same intermediate, activation of the 2nd C–H bond of methane occurs *via* TS3′ to give CH_2 and water (IM6′). All the transition states are also verified by the IRC, which connects the respective reactant and product. The distances of the Pd atom from the framework oxygen atoms are shown in Table S5.

To gain insight into the thermodynamic view of the reaction pathway, the potential energy surface (PES) diagram of Gibbs free energy (kcal mol^{-1}) *vs.* reaction coordinate is plotted and is shown in Fig. 2. The PES is calculated with reference to the reactants, *i.e.*, Pd@ZSM-5 + N_2O + CH_4, which is carried out at 298 K and 1 atm pressure. From Fig. 2, it has been observed that the overall reaction is spontaneous and thermodynamically favorable. The N_2O adsorption step is spontaneous with a free energy of -10.18 kcal mol^{-1}. However, the N–O dissociation TS (TS1) is endoergic and non-spontaneous with an activation barrier (IM1 → TS1) of 21.96 kcal mol^{-1}. With a desorption energy of 4.65 kcal mol^{-1}, the N_2 gas is easily removed from the system to form active species (IM3) with a relative free energy of 3.04 kcal mol^{-1}. The methane adsorption step is quite endoergic with a relative free energy of 14.34 kcal mol^{-1}, which could be attributed to the confinement effect of ZSM-5 microspores.[91] This less stable adsorption of methane also facilitates the 1st C–H activation of methane with an activation barrier of merely 0.12 kcal mol^{-1} (IM4 → TS1) and a relative free energy of 14.46 kcal mol^{-1}. The complete breakdown of the C–H bond results in a highly stable intermediate with a free energy of -40.73 kcal mol^{-1}. The stability of the intermediate is due to the coordination of Pd to the O atom of the zeolite's framework including the confinement effect. After this intermediate, the feasibilities of the pathways mentioned are determined in terms of their activation barrier in the PES. As shown in Fig. 2, the activation energy of CH_3–OH recombination is much lower compared to the 2nd C–H bond activation of methane that leads to the formation of H_2O and the Pd–CH_2 moiety. The NBO second order perturbation analysis offers a distinct electronic explanation for why the CH_3–OH recombination pathway (TS3) is favored over the 2nd C–H activation pathway (TS3′). A significant interaction of the Pd lone pair with the antibonding σ*(O–C) ($E^{(2)}$ = 22.7 kcal mol^{-1}) suggests effective overlap between Pd d orbitals and formation of the C–O bond in TS3, which leads to the stabilization of the transition state. The enhanced donor acceptor stabilization in TS3 accounts for the reduced energy barrier of methanol production compared to that of the 2nd H abstraction. Desorption of methanol from the framework system post-formation is critical, since elevated desorption energy may lead to the over oxidation of methanol. In the Pd@ZSM-5 system, methanol is easily desorbed from the system with a minimum energy of 10.57 kcal mol^{-1}, making it a viable process and

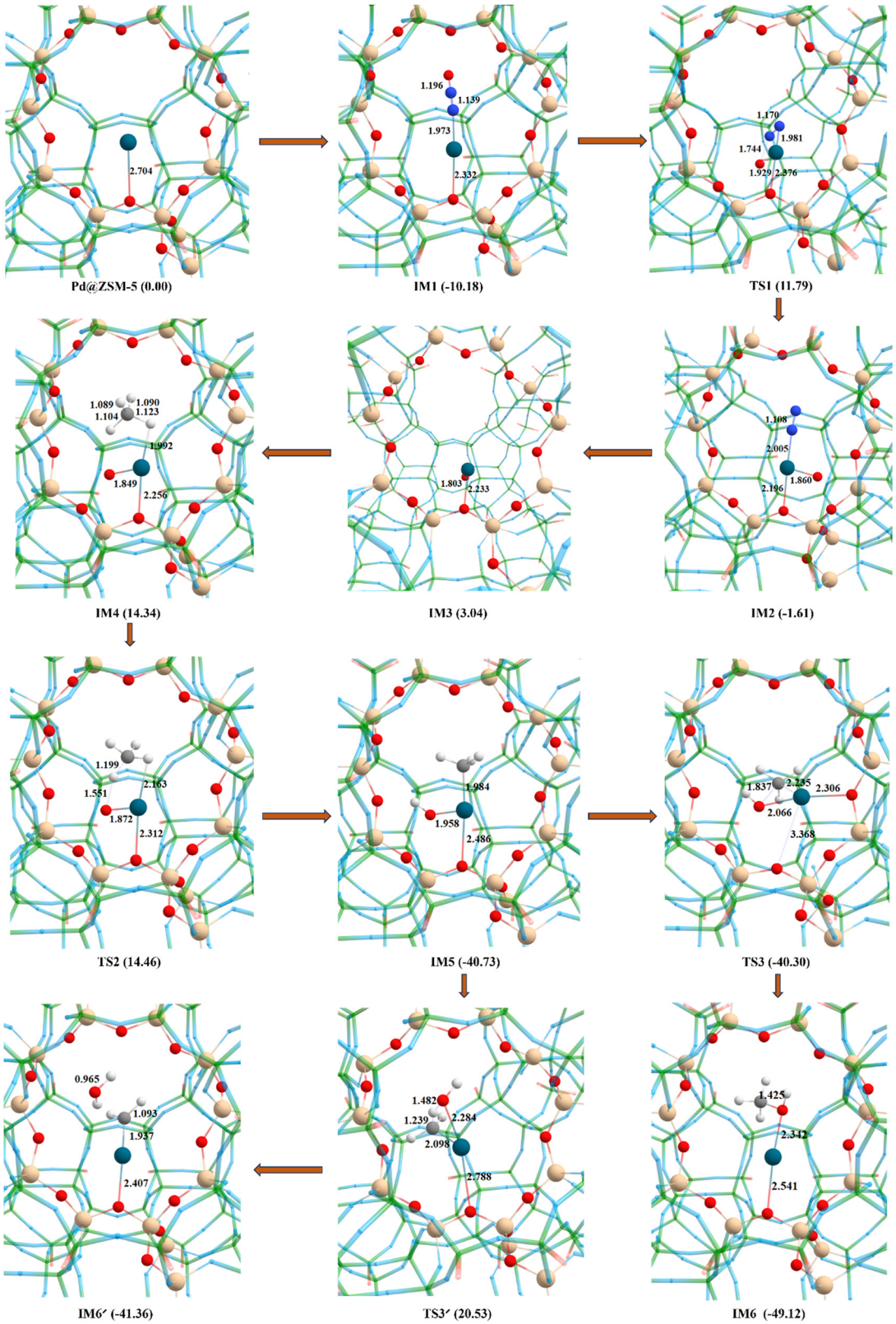

Fig. 1 Optimized diagrams involved in the partial oxidation of methane with Pd@ZSM-5 obtained from ONIOM calculations (relative Gibbs free energy of each step is given in parentheses).

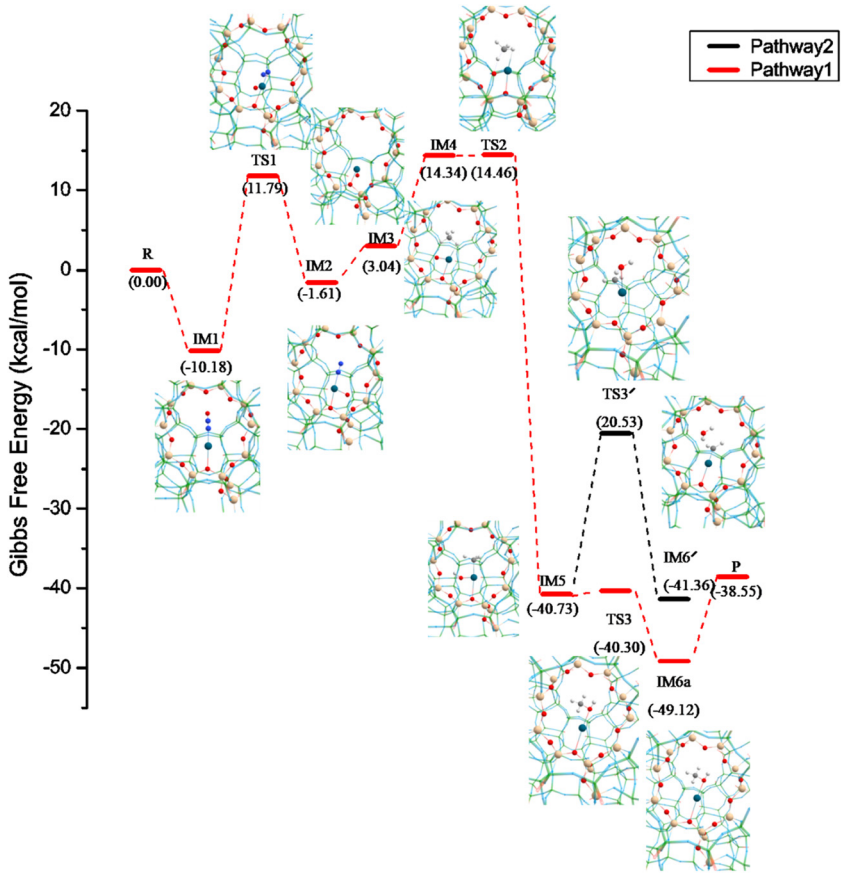

Fig. 2 PES of partial oxidation of methane to methanol and carbene, water.

preventing over oxidation to unnecessary products like CO_2, CO, *etc.* This observation is supported by the weak donor–acceptor interaction between Pd and the methanol molecule as well as a Wiberg bond index value of 0.12 for Pd–$OHCH_3$. We have also calculated the desorption of methanol in the presence of water in the system; however, the energy changes by only 1.09 kcal mol^{-1}. Thus, adsorption of water molecules does not significantly affect the environment of the siliceous zeolites due to the hydrophobic nature of the siliceous zeolites.[92] The PES diagram of methanol desorption with and without the addition of water molecules in the system is shown in Fig. S5. The activation barrier of the transition states involved in the pathway is tabulated in Table 1 and the imaginary vibrational frequencies of the transition states are shown in Table S9.

Table 1 Activation barrier for all the transition states involved in the reaction pathway

	Activation energy (kcal mol^{-1})			
Catalyst	N–O (TS1)	C–H (TS2)	CH_3–OH (TS3)	CH_2–OH_2 (TS3′)
Pd@ZSM-5	21.96	0.12	0.43	20.20
Pd^+@ZSM-5	41.2	6.51	10.39	23.40
$^1Pd^{2+}$@ZSM-5(ori2)	50.69	13.58	17.12	46.86
$^3Pd^{2+}$@ZSM-5 (ori2)	4.39	7.35	22.11	5.13
$^3Pd^{2+}$@ZSM-5 (Al–O–Si–O–Si–O–Al)	3.81	15.23	19.34	29.79

Partial methane oxidation to methanol using Pd^+@ZSM-5

In this section, we discuss the active site formation and partial oxidation of methane to methanol by Pd^+@ZSM-5. To gain a deeper understanding of the electronic environment and reactivity in Pd^+@ZSM-5, the Si atom at the T12 site is replaced by an Al atom to create a localized negative charge that electrostatically balances the cationic Pd center as illustrated in Fig. S1. The frontier molecular analysis reveals that Pd^+@ZSM-5 is an open shell configuration with the HOMO and the LUMO lying in the β orbitals, primarily dominated by the 4d-orbitals of the Pd atom. With small $4d_{yz}$ and $4d_{xz}$ contributions, the HOMO consists of mostly the $4d_{z^2}$ orbital of Pd, whereas the LUMO is mainly localized on the $4d_{xy}$ of Pd and antibonding $2p_y^*$ orbitals of framework oxygen atoms as shown in Fig. S2. This orbital distribution indicates a metal center donor–acceptor duality, with d_{z^2} functioning as the σ donor for the electrophilic substrates and the d_{xy} orbital serving as the π-acceptor. The lower natural charges on the Pd atom (0.719*e*) than the formal oxidation state indicate polarization as well as covalency, which is also consistent with the previous literature.[93] The various modes of the metal encapsulation are shown in Fig. S6 and it is found out that the one near the Al atom is the most stable, highlighting the role of framework charge in anchoring the active site.

The optimized diagrams involving intermediates and transition states are shown in Fig. 3 along with the potential energy surface (PES) in Fig. 4. The initial orientation and binding mode of a reactant molecule at the catalyst surface significantly influence the reaction pathway and kinetics.[94] Therefore, we have calculated the adsorption of N_2O from both N-terminal and O-terminal sides to find the appropriate starting material for the reaction to proceed.

As in the preceding section, the reaction commences with the adsorption of N_2O onto Pd^+@ZSM-5. As shown in Fig. 4, the adsorption process is spontaneous with an adsorption energy of -18.19 kcal mol^{-1}. N_2O is adsorbed on Pd^+@ZSM-5 (IM1a) with a Pd–N distance of 2.143 Å, which is accompanied by the charge distribution, as indicated by the reduction in Pd charge (0.719*e* to 0.669*e*) and the accumulation of the negative natural charge in N ($-0.224e$). The charge separation weakens the N–O bond, leading to its elongation from 1.176 Å in IMa to 1.625 Å in TS1a. In the transition state, the O atom moves closer to the Pd atom to further elongate Pd–N and form the interaction between Pd and O. The single imaginary frequency of 609.72*i* of TS1 is verified from IRC calculations. In IM2a, N–O completely dissociated to form Pd–O and Pd–N_2 bonds with bond lengths of 1.859 Å and 2.028 Å respectively. The natural charges on Pd (0.709) and O (-0.357) along with the spin densities (Pd = 0.087, O = 0.933) suggest that the unpaired electron is on the O atom, which aligns with the formation of a Pd–O$^\bullet$ radical like intermediate. By eliminating N_2 from IM3a, we have obtained the active species Pd–O with a bond distance of 1.804. In IM3a, the Pd atom carries a natural charge of 0.876 and the O atom retains a similar charge -0.348 but the spin density on the Pd atom decreases to 0.017 and that of O increases to 1.001. Such a change in spin density reflects the complete transfer of electron density from Pd to O. This resultant high spin density on the reactive O atom is crucial for the activity of the metal encapsulated zeolites.[95] The methane molecule adsorbs on the active species (IM4a) with an adsorption energy of -32.05 kcal mol^{-1}, which is highly stable compared to the adsorption of methane on the siliceous zeolites. The methane adsorption leads to the partial reduction of the Pd atom (0.876 → 0.779) due to the σ(C–H) donation to the lp*(Pd). At the same time, the O atom exhibits a slightly more negative charge (-0.374), resulting in a slightly polarized $Pd^{\delta+}$–$O^{\delta-}$ pair that could promote C–H bond activation. The spin density value of 0.908 on the O atom shows that the electron density remains localized in the O-atom, making it a reactive center for H-abstraction. Eventually the activation of the C–H bond of methane proceeds *via* TS2a with a single imaginary frequency of 1061.13*i* cm^{-1}. In TS2a, the C–H bond elongated to 1.271 Å and the H–O bond forms with a distance of 1.372 Å. The delocalization of spin is observed from the O to Pd and H, which is consistent with the partial electron sharing rather than complete charge transfer. As a result of this homolytic C–H activation, Pd–CH_3 and Pd–OH bonds formed (IM5a) with a distance of 2.003 Å and 1.890 Å, respectively. The spin density (Pd = 0.558 and O = 0.430) indicates that the unpaired electron, which is initially located on the O-atom, becomes partially located on Pd that completes the H-abstraction. Similar to the previous section, we have explored two possibilities of product formation, namely, pathway 1 and pathway 2 starting from IM5a. In pathway 1, the recombination of the CH_3 and OH moieties occurs through TS3a, where the formation of the C–O bond begins with a bond distance of 2.034 Å. With a single imaginary frequency of 445.34*i* cm^{-1}, TS3a connects IM5a and the desired product methanol in IM6a. Instead of the formation of the C–O bond, in pathway 2 we have explored the possibility of activation of the 2nd C–H bond of methane *via* TS3a′. As a result, we have obtained the CH_2 moiety and the H_2O molecule in IM6a′ as shown in Fig. 3, which are attached to the Pd atom with a distance of 2.109 Å and 2.251 Å respectively. It has been observed that the distance between the encapsulated Pd atom and the framework O-atoms varies in the range of 2.029 to 2.400 Å during the reaction process. The variation in bond lengths reflects the change in the electron density of the Pd atom, activation, dissociation and formation of various bonds during the reaction cycle. The changes in the bond lengths of Pd with framework O-atoms during the reaction cycle are shown in Table S6.

Comprehending the principal characteristics of the potential energy surface might facilitate the identification of the factors influencing the activity of Al-substituted ZSM-5 in the methane oxidation reaction. The minimum energy pathway for methane oxidation on Pd^+@ZSM-5 is shown in Fig. 4 to understand the thermodynamic prospect of the reaction mechanism. All the energies are calculated with respect to Pd^+@ZSM-5 + N_2O + CH_4 at 1 atm pressure and 298 K temperature. The overall reaction is spontaneous and exoergic as shown in the figure. The N_2O adsorption step (IM1a) is spontaneous and thermodynamically feasible (E_{N_2O}, -7.76 kcal mol^{-1}). The activation barrier of N–O dissociation (IM1a → TS1a) is comparatively high (41.2 kcal mol^{-1}), establishing O-transfer as the turnover controlling event. Upon O_2 transfer, N_2 is easily removed from the system (E_{des} = -0.95 kcal mol^{-1}), which is consistent with the spin density distribution. As the spin density is mainly localized on the Pd atom (0.089) and negligible on N atoms (-0.002) N_2 can easily be removed from the system as no significant interaction was formed between them in IM2. Unlike in the case of siliceous zeolites, methane adsorption in the Al-substituted ZSM-5 is highly stable and spontaneous with a relative energy of -24.19 kcal mol^{-1}. Previous studies on the experimental values of the methane adsorption also support the finding that methane demonstrated enhanced binding in Al-ZSM-5 compared to the solely siliceous variant.[96] The activation of the C–H bond of methane is also found to be spontaneous and has an activation barrier of 6.51 kcal mol^{-1}. The activation barrier is consistent and even lower compared to some previous studies.[97,98] The resulting homolytic product is situated at -50.69 kcal mol^{-1} lower than the reactants. The stability of the intermediate is due to the delocalization of spin density over mainly Pd and non-framework or active oxygen species and also due to the non-radical type behavior of CH_3 and OH species. The intermediate is structurally anchored as well as electronically stabilized. Two reaction channels compete from this state. In pathway 1, the recombination of CH_3 and OH occurs with a barrier (IM5a → TS3a) of 10.4 kcal mol^{-1}, which results in the formation of methanol

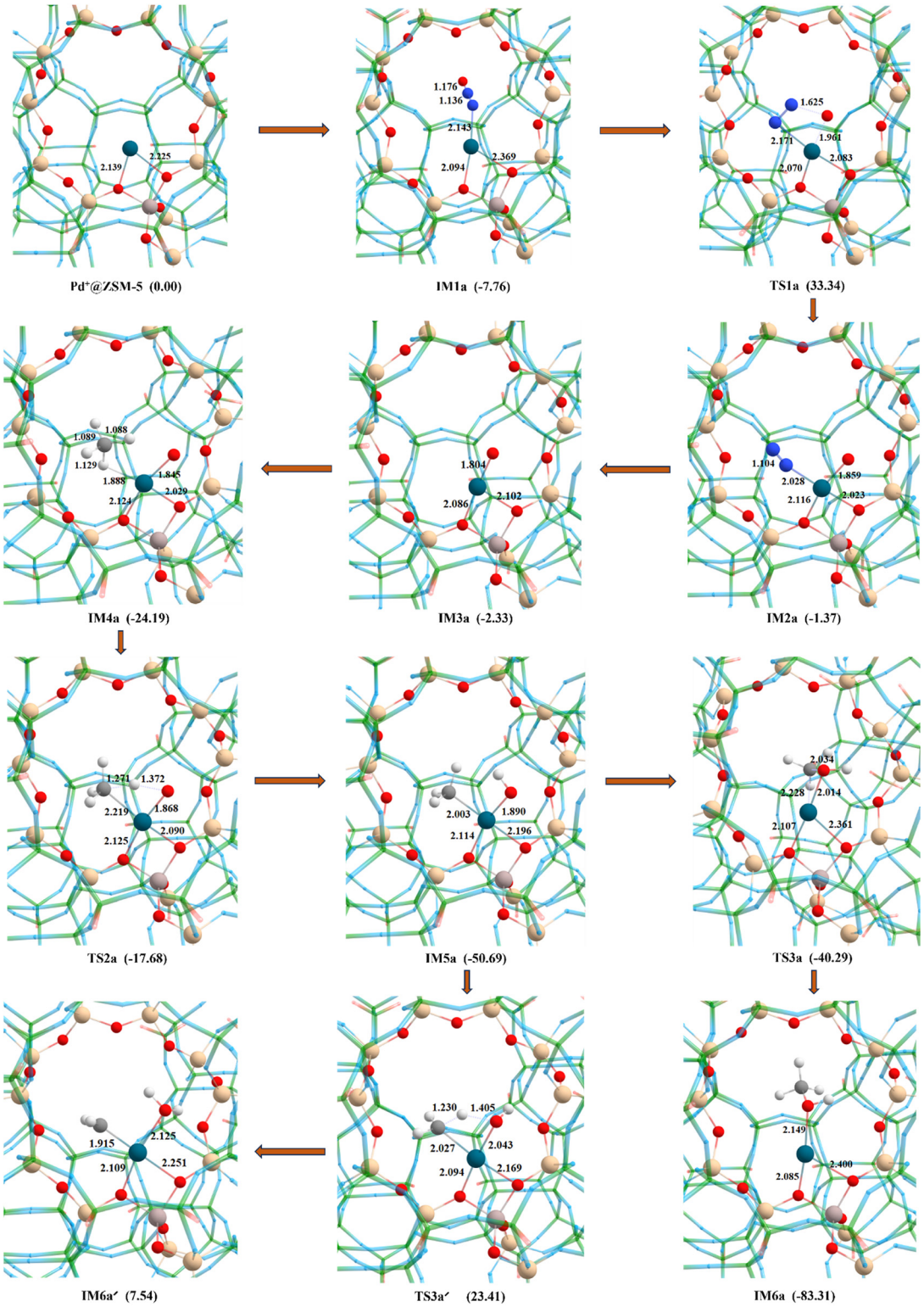

Fig. 3 Optimized diagrams involved in the partial oxidation of methane with Pd^{+}@ZSM-5 obtained from ONIOM calculations (relative Gibbs free energy of each step is given in parentheses).

favored both kinetically and thermodynamically. In pathway 2, activation of the 2nd C–H bond requires a higher energy barrier (IM5a → TS3a′) of 23.40 kcal mol^{-1}, confirming that 1st C–H activation followed by the CH_3–OH recombination is the primary path. The desired product methanol exhibits highly exergonic nature (ΔG = −83.3 kcal mol^{-1}); however, this leads to the requirement of a desorption energy of 44.76 kcal mol^{-1}. This high stabilization is reflected due to the pronounced charge

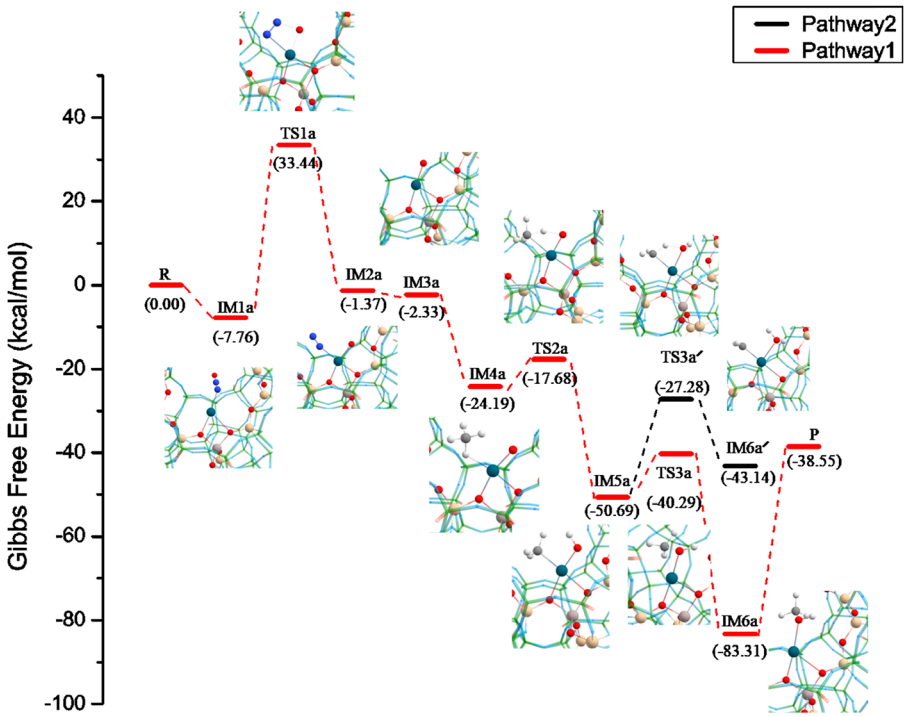

Fig. 4 PES of partial oxidation of methane to methanol and carbene, water.

transfer from the lone pair of O(–HCH_3) to the antibonding orbital of the Pd–O bond. However, this value is quite high and may often lead to over-oxidation of methanol. Therefore, we have also calculated desorption of the methanol molecule while adding additional water molecules in the system.[22,99] The PES diagram of desorption of the methanol molecule from Pd^{+}@ZSM-5 with and without ZSM-5 is shown in Fig. S7. From the figure, it has been observed that addition of water molecules drastically lowers the desorption energy of methanol compared to the one with the absence of water molecules. The water molecule forms a strong bond with a distance of 2.114 Å with the Pd atom, thus acting as a competitor for the methanol molecule, which is adsorbed at the same Pd atom. Consequently, the interaction between methanol and the palladium atom diminishes as the presence of an extra water molecule reduces desorption of methanol from the system. In comparison to siliceous zeolites, Pd@Al-ZSM-5 shows a considerable effect of water molecules on methanol desorption.

Partial methane oxidation to methanol using Pd^{2+}@ZSM-5

In the previous two sections we have discussed the active site formation and partial oxidation of methane to methanol using siliceous ZSM-5 and Al substituted ZSM-5 where the formal charge of the Pd atom is 0 and +1 respectively. In this section we have used a divalent Pd cation with formal charge +2 to study how active site reactivity and overall reaction parameters change during the conversion process. We have replaced two Si atoms with two Al atoms to maintain the overall charge neutrality of the ZSM-5 framework.[100] With respect to cluster model representation of the ZSM-5 framework, the modes of Al substitution are shown in Fig. S8. Although additional positions for Al substitution are available, the focus on the reaction mechanism of the methane oxidation process enhances the clarity and coherence of the discussion. Therefore, we have considered only two positions to demonstrate the overall reaction mechanism. The molecular orbital HOMO–LUMO of the proposed Pd^{2+}@ZSM-5 framework is shown in Fig. S2. The HOMO of the closed shell singlet species is delocalized on the non Pd bonded Al atom ($3p_z$), $2p_z$ of framework O atom and $4d_{xy}$ of Pd atom, while the LUMO is on the $4d_{xy}$ and $4d_{yz}$ of the Pd atom. The system is more delocalized with Pd-framework electronic coupling. We can also observe that the Al atom which is not directly bonded to the Pd atom influences the frontier orbital, indicating long range electronic effects throughout the zeolite cluster. In the triplet spin state, the HOMO is mainly localized on the $4d_{z^2}$, $4d_{yz}$ orbital of the Pd atom as well as the $2p_y$ orbital of framework O atoms adjacent to the Al atoms. On the other hand, the LUMO is on the $3p_x$ orbital of the non-Pd bonded framework Al atom, suggesting the active involvement of framework electrons as shown in Fig. S2. This indicates that distinct reaction pathways may exist for singlet and triplet spin states.

As the energy difference of the ground singlet state and the 1st excited triplet state is not very high, we have considered two-state reactivity.[101,102] The optimized structures of the intermediates and the transitions states involved in the singlet and triplet pathways are shown in Fig. 5 and 6, respectively. While the pathway from methane to methanol is identical in both spin states, the modes of N_2O adsorption differ between them; thus, both pathways are illustrated here. For the ground state singlet species, the N_2O adsorption is calculated both *via*

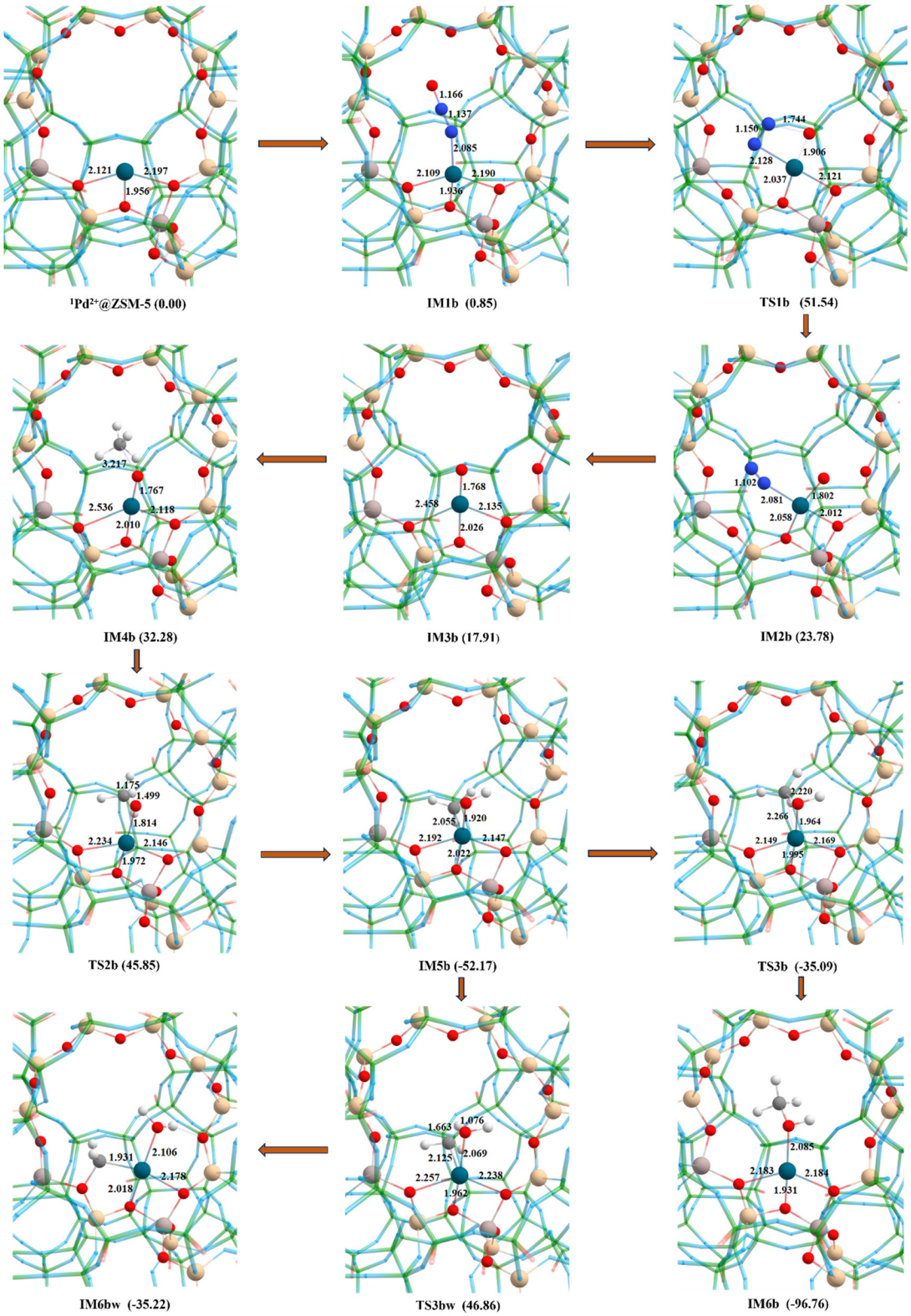

Fig. 5 Optimized diagrams involved in the partial oxidation of methane with Pd^{2+}@ZSM-5 at a singlet spin state obtained from ONIOM calculations.

N-terminal and O-terminal sides, as shown in Fig. S9. Adsorption is favorable in both cases with only a small energy difference; the N-terminal side is slightly more stable. The terminal nitrogen in N_2O possesses a lone pair in a more diffuse orbital, rendering it more polarizable, thus a softer base than the O-terminal, which is harder due to greater electronegativity and denser electron distribution. Owing to its soft Lewis acid nature, the orbital interaction between N-terminal

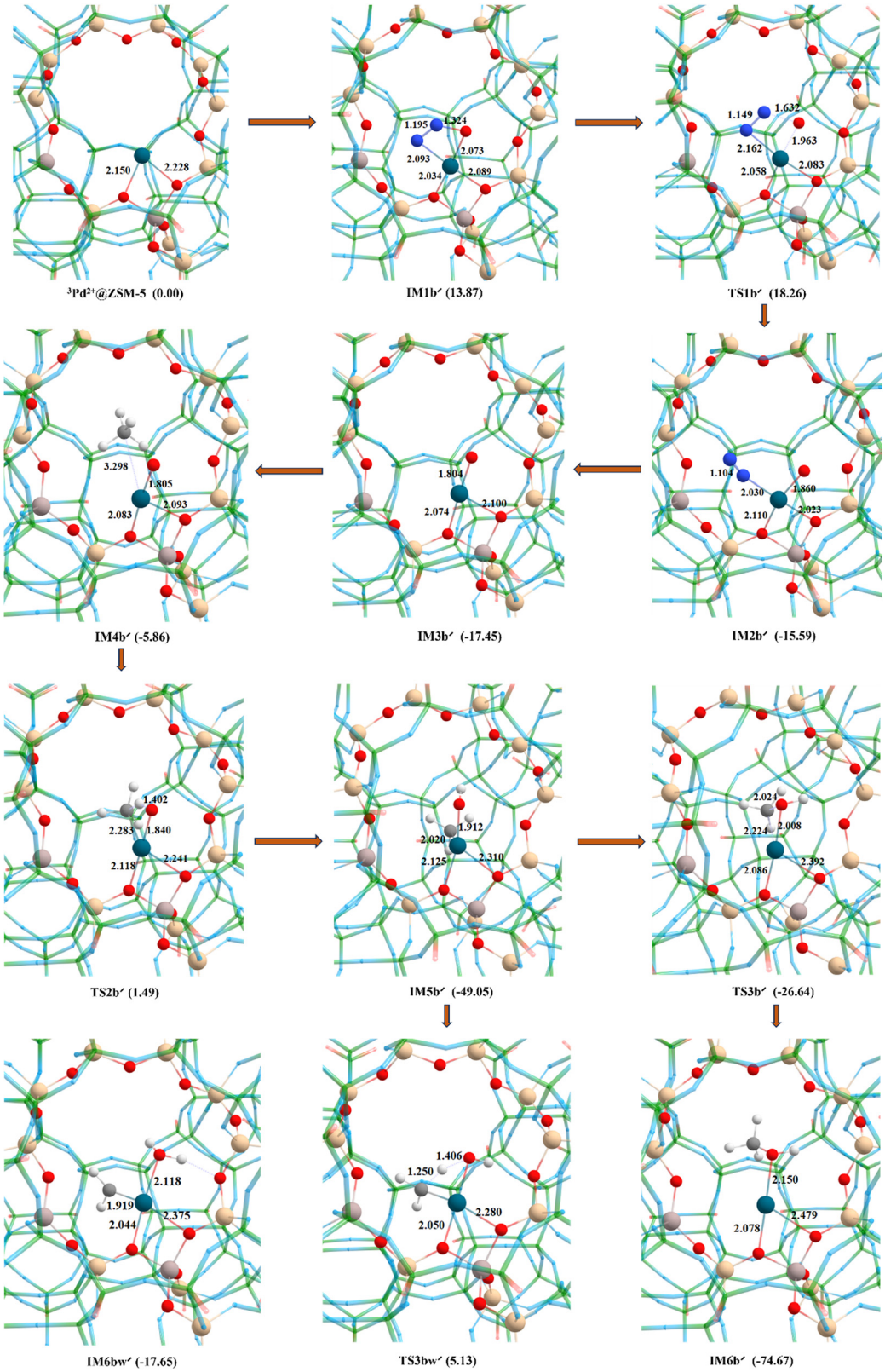

Fig. 6 Optimized diagrams involved in the partial oxidation of methane with Pd^{2+}@ZSM-5 at a triplet spin state obtained from ONIOM calculations.

and Pd^{2+} is energetically more favorable. NBO analysis also offers quantitative evidence for the preference of the N-terminal adsorption mode. The key donor–acceptor interaction of lp(N) → lp(Pd)* exhibits a stabilization energy twice the value of that of lp(O) → lp(Pd)*. Thus, the reaction is further investigated with the N terminal modes of adsorption of N_2O.

In Fig. 5, the Pd atom is coordinated with three framework O-atoms of the ZSM-5 cluster. The bond distances of the active center with framework atoms are shown in Table S7. Following the N-terminal adsorption (IM1b), the Pd–N bond forms with a distance of 2.085 Å, exhibiting only slight changes in the N–N bond length at 1.137 Å and the N–O bond length at 1.166 Å, indicating donor coordination rather than direct activation. In IM1b, the natural charge of the Pd atom reduces from 0.838*e* to 0.780*e* and the O atom gains a charge of −0.204*e*. At the transition state TS1b (629.96*i*), N–N and N–O bond lengths elongated respectively to 1.150 Å and 1.744 Å, while Pd–O bond formation takes place with a bond length of 1.906 Å. During the TS1b, the Pd atom slightly oxidizes (0.810*e*) and the O atom gains more negative charge (−0.382*e*), consistent with the O transfer process. In IM2b, complete dissociation of the N–O bond leads to the formation of Pd–O with retention of N_2 with a bond length of 1.102 Å. The Pd–O interaction in IM2b transitions from donor–acceptor coordination to a pure σ-type bond by the strong orbital overlap between the 4d orbital of Pd and 2p of the O atom. During the release of N_2 in IM3b, Pd reoxidises (1.107*e*), generating the Pd–O active centre. Methane is initially adsorbed through physisorption in intermediate IM4b, characterized by a C–O distance of 3.217 Å and weak donor acceptor overlap, indicating weak van der Waals interactions with the active site. As the reaction progresses, the σ(C–H) of the methane bond interacts strongly with the PdO active site. Subsequently, C–H bond activation occurs *via* the transition state TS2b, which exhibits a single imaginary frequency of –1358.67*i* cm^{-1}. At this stage, the C–H bond elongates to 1.175 Å, while a new H–O (Pd) bond forms with a bond length of 1.499 Å. In TS2b, the σ(C–H) bonding orbital contributes electron density to the antibonding Pd–O orbitals, thereby diminishing the C–H bond and promoting its cleavage. The delocalization reduces the strength of the σ(C–H) bond without directly populating its antibonding orbital, aligning with a concerted, homolytic activation mechanism. After breaking of the C–H bond, the methyl fragment coordinates with the Pd center, while the H atom attaches to the active O atom, forming a hydroxyl group in IM5b. Similar to Pd@ZSM-5 and Pd^{+}@ZSM-5, here we have moved towards two transition states to get two different products. The optimized diagrams of the intermediates and transition states are shown in Fig. 5. Methanol formed in IM6b *via* the TS3b, where CH_3 and OH recombine with a single imaginary frequency of 423.16*i* cm^{-1}. In the other path, water and the CH_2 group formed *via* TS3bw as shown in Fig. 5. All the imaginary frequencies associated with the reaction mechanism are presented in Table S9.

A similar reaction pathway with identical key steps is observed for the $^3Pd^{2+}$@ZSM-5 system, as shown in Fig. 6. In contrast to $^1Pd^{2+}$@ZSM-5, where N_2O binds in a linear fashion, the molecule adopts a bridged coordination mode in $^3Pd^{2+}$@ZSM-5, interacting through both nitrogen and oxygen atoms. Despite the more extended coordination, the adsorption energy in $^3Pd^{2+}$@ZSM-5 is slightly endothermic at +2.11 kcal mol^{-1}, compared to the more favorable exothermic value of –10.01 kcal mol^{-1} in $^1Pd^{2+}$@ZSM-5. This difference can be attributed to the spin multiplicity and resulting electronic configuration in $^3Pd^{2+}$@ZSM-5, which may lead to reduced orbital overlap or destabilizing spin-state interactions during adsorption, making the bridged mode less energetically favorable despite its geometric adaptability. In the O-transfer process (IM1b′ → TS1b′ → IM2b′) there is gradual shift of electron density from N_2O to the Pd–O unit. The elongation of the N–O bond from 1.324 Å to 1.632 Å (TS1b′) results in a gradual localization of spin density on the O-atom, which enhances its radical like reactivity, and subsequently makes the N–O dissociation feasible. In IM2b′ the N–O bond is completely dissociated with spin density localized on the O atom. This localization is further intensified following the removal of N_2 from the system in IM3b′. With an endothermic adsorption of energy of 4.36 kcal mol^{-1}, methane physisorbed onto PdO@ZSM-5 through van der Waals interaction. Weak donor–acceptor interaction was observed between σ(C–H) and Pd(d) orbitals in IM4b′. As the reaction proceeds towards TS2b′, activation of the C–H bond takes place, where the C–H bond elongates to 1.275 Å and the O–H bond starts to form with a bond distance of 1.406 Å, as shown in Fig. 6. During the process, the enhanced σ(C–H) →lp*(O) and σ(C–H) →BD*(Pd–O) facilitates the electron delocalization to weaken the C–H bond of methane. The completely activated C–H bond creates one CH_3 group, which attaches to Pd, and the O atom abstracts the H atom to form the OH group in IM5b′. Similar to all the previous cases, the mechanism is carried out in two directions to get two different products. All the vibrational frequencies involved in the transition states are shown in Table S9.

Fig. 7 shows the potential energy diagram of the partial oxidation of methane to methanol, with comparison of singlet and triplet spin states. The ground spin state, which is the singlet spin state of Pd^{2+}@ZSM-5, was used as a point of reference for constructing the potential energy surface (PES) at 298 K temperature and 1 atm pressure. Both the spin states exhibit an exoergic reaction profile but the individual steps differ in energetics. For the singlet spin, the free energy of N_2O adsorption is slightly endothermic (0.85 kcal mol^{-1}) followed by kinetically demanding N–O dissociation (IM1b → TS1b) with significant energy barrier. The overall activation step is also non-spontaneous with a relative energy of 23.78 kcal mol^{-1} in IM2b. The N_2 gas is easily desorbed from the system with a desorption energy of −5.86 kcal mol^{-1}. Methane is adsorbed with a relative free energy of 32.28 kcal mol^{-1}, and its subsequent C–H activation (IM4b → TS2b) proceeds through a favorable barrier of 13.57 kcal mol^{-1}. The product from methane activation (IM5b) is a highly stabilized intermediate (ΔG = −52.17 kcal mol^{-1}), which aligns with the charge delocalization occurring between the Pd center and the Brønsted acidic framework. The desired product of methanol recombination (IM5b → TS3b) has the activation barrier of 17.12 kcal mol^{-1}. The PES containing comparison of CH_3–OH recombination (IM5b → TS3b) and 2nd C–H activation (IM5b → TS3bw) in $^1Pd^{2+}$@ZSM-5 is shown in Fig. S10. The activation barrier is much higher for 2nd C–H activation compared to the methanol production, making the desired reaction feasible. The desorption of methanol from the metal–framework system requires 58.22 kcal mol^{-1}; however, introducing a water

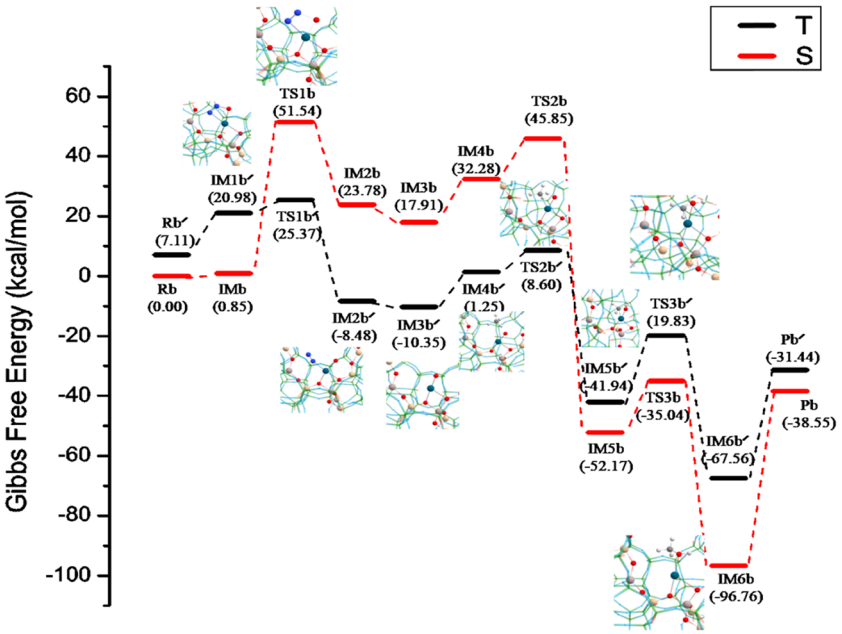

Fig. 7 PES of partial oxidation of methane to methanol *via* singlet and triplet states on Pd^{2+}@ZSM-5.

molecule significantly reduces this energy barrier, as water competes with methanol for coordination at the Pd active site. The lowering of desorption energy of methanol in the presence of one additional water molecule is shown in Fig. S11.

The triplet spin state of the reactant species is calculated to be 7.11 kcal mol^{-1} higher in energy relative to its singlet counterpart. Although N_2O adsorption in the triplet state is more endothermic than that in the singlet state, the subsequent N–O bond dissociation proceeds with a lower activation barrier of 4.39 kcal mol^{-1}, rendering the triplet pathway more favorable. The dissociation process is spontaneous, leading to an intermediate (IM2b′) with a relative free energy of –8.48 kcal mol^{-1}. This is followed by a barrierless desorption step that generates the active center (IM3b′) onto which methane adsorbs to form IM4b′ with a relative free energy of 1.25 kcal mol^{-1}. Notably, the overall pathway from N–O bond dissociation to methane adsorption follows the lowest energy route in the triplet spin surface. The spin density analysis of the transition state (TS1b′) reveals a moderate localization of unpaired electron density on the oxygen atom (0.553), indicative of emerging radical character as the N–O bond begins to dissociate. The low spin density on the Pd center (0.07), on the other hand, indicates little spin delocalization to the metal and is consistent with a homolytic cleavage mechanism, where the oxygen primarily retains the unpaired electron. Subsequent to bond dissociation, the resultant intermediate (IM2b′) demonstrates a markedly increased spin density on oxygen (0.933). In the intermediate IM3b′, the oxygen atom displays a spin density of 1.029, signifying a completely localized unpaired electron and validating the existence of a terminal oxyl radical. After methane adsorption, the oxygen spin density in IM4b′ stays high at 1.013, indicating that the system maintains its triplet open-shell configuration. Methane C–H bond activation proceeds *via* a transition state with an energy barrier (IM4b′ → TS2b′) of 7.35 kcal mol^{-1}, which is 6.22 kcal mol^{-1} lower than that observed in the singlet state. During the TS2b′, spin density on the O atom decreases, indicating that the radical is partially quenched as it begins to abstract the H atom from methane. Simultaneously, the spin density on the Pd center rises to 0.227, indicating that the metal is now more involved in stabilizing the unpaired electron. The resulting product of methane activation (IM5b′) in the triplet state lies higher in energy, with a relative free energy of −41.94 kcal mol^{-1}, as illustrated in Fig. 7. The methanol formation step has an activation barrier (IM5b′ → TS3b′) of 22.10 kcal mol^{-1}, which is higher than that of the 2nd C–H activation step (IM5b′ → TS3bw′), as shown in Fig. S12. From Fig. 7, it has been observed that for the 1st half of the reaction up to the C–H activation step, the triplet spin state is preferred, whereas for the later part of the reaction singlet spin dominates the pathway as it is the lowest energy pathway. After the formation of IM5b′, representing the product of methane C–H bond activation on the triplet surface, the reaction profile indicates a divergence in spin-state preference based on the succeeding step. Despite the substantial stabilization of IM5b′ (−41.94 kcal mol^{-1}) in the triplet configuration, the methanol formation step (IM5b′ → TS3b′) encounters a considerable activation barrier of 22.10 kcal mol^{-1} on the triplet surface. This suggests that the transformation is more advantageous on the singlet spin surface, where orbital pairing and bond formation between CH_3 and OH are more effective. Conversely, the second C–H activation step (IM5b′ → TS3bw′) is more advantageous in the triplet state, evidenced by a reduced energy barrier relative to the singlet pathway as well as methanol formation. This indicates persistence of the radical-type reactivity stabilized by the triplet spin structure. This behavior highlights the significance of spin-state flexibility in the catalytic cycle and aligns with established patterns of two-state or multi-state

reactivity, where several steps occur along separate spin surfaces to get the lowest energy pathway.[14] The PES of desorption of the methanol molecule with and without the water molecule is shown in Fig. S13.

We further investigated the mechanism of the methane oxidation reaction by exploring an alternative orientation for the substitution of the second Al atom within the 10-membered ring of the zeolite framework, as depicted in Fig. S14. In this case, the Al–O–Si–O–Si–O–Al connectivity was considered on both sides relative to the T12-substituted Al atom. Our results indicate that the triplet spin state remains the ground spin state for both orientations. As shown in the HOMO–LUMO diagram in Fig. S15, the HOMO is entirely localized on the d_{z^2} orbital of the Pd atom, whereas the LUMO is primarily situated on the second Al atom. This contrasts with the previously studied configuration, where the LUMO was delocalized over both the Pd atom and the second substituted Al site. The HOMO in $4d_{z^2}$ and $4d_{yz}$ signifies the availability of electrons in the Pd orbital for donation to the incoming reactant molecules.

Fig. 8 shows the optimized diagrams for the methane oxidation process using the mentioned Pd^{2+}@ZSM-5 catalyst with different Al substitution than the previous one. Here the Pd atom is η^2 coordinated to two of the framework O-atoms, ensuring electronic stabilization. The bond lengths of the Pd atom with the framework O-atom during the reaction process is shown in Table S8. Adsorption of N_2O in IM1d in a bridging manner leads to the pre activated complex, where the N–O bond weakens prior to the dissociation process. The strong donor–acceptor interaction between lp(O) → σ*(N–N) and lp(O) → σ*(O–Pd) promotes the charge delocalization within the complex. Also, the lp(N) → lp*(Pd) interaction enhances the electron backdonation to the Pd center, making it more reactive to the O transfer process. In TS1d (−611.84*i*) movement of electrons mainly occurs through the σ*(N–N) →σ*(N–O) and lp(N) → lp*(Pd) interactions, which indicate the role of Pd in the N–O cleavage process. Desorption of the N_2 gas from the system results in the formation of oxo-like active species (IM3d) with a Pd–O bond length of 1.804 Å. In IM3d, the natural charge on the Pd atom slightly increases to 0.873*e*, while that of O possesses −0.345*e*, indicating charge delocalization between two atoms. Physisorption of methane takes place in IM4d, where methane engages with a weak interaction with the Pd–O active site. The activation of the 1st C–H bond of methane proceeds *via* TS1d with a single imaginary frequency of 1603.14*i* cm^{-1}. At this point, the C–H bond in TS2d transitions to activate with a length of 1.322 Å, and the O–H bond starts to develop with a length of 1.197 Å. The interaction of lp(O) → σ*(C–H) observed in NBO analysis confirms the strong donor–acceptor coupling responsible for the activation. Complete activation of the C–H bond leads to the formation of IM5d with formation of Pd–CH_3 and Pd–OH bonds with a distance of 2.019 Å and 1.911 Å respectively. After the formation of IM5d, two pathways have been studied just like in the previous cases. With a single imaginary frequency of 450.46*i* cm^{-1}, recombination of CH_3 and OH moieties takes place *via* TS3d to finally form the desired product methanol in IM6d with the Pd–$OHCH_3$ distance of 2.144 Å. In another pathway 2, the activation of the 2nd C–H bond of methanol occurs *via* the TS3d′ characterized by a single imaginary frequency of 1703.82*i* cm^{-1} to form Pd–CH_2 and water as shown in Fig. 8.

Fig. 9 shows the PES diagram of the partial oxidation of methane using the Pd^{2+}@ZSM-5 catalyst with the Al–O–Si–O–Si–Al–O linkage to investigate how the energetics changes upon the substitution of the 2nd Al atom in different positions. The Gibbs Free energies are calculated with respect to the triplet spin state, which is the ground state of the mentioned catalyst. The adsorption of N_2O is significantly endothermic by 17.92 kcal mol^{-1}, accompanied by the Gibbs free energy of 29.70 kcal mol^{-1}. This suggests that while the step is thermodynamically unfavorable, it remains kinetically feasible. Following adsorption, the N–O bond readily undergoes dissociation with an activation energy (IM1d → TS1d) of 3.81 kcal mol^{-1}, resulting in the formation of the Pd–O intermediate and release of N_2 with barrierless desorption (IM2d → IM3d, −0.99 kcal mol^{-1}). In IM3d, the HOMO is localized mainly on the $4d_{xz}$ and $4d_{x^2-y^2}$ of Pd and $2p_y$ of the O atom, indicating the strong Pd–O orbital interaction that contributes to the oxidizing character of the active site. The adsorption energy of methane is exothermic (−10.70 kcal mol^{-1}) and the process is spontaneous with a relative free energy of −6.79 kcal mol^{-1}. The activation of the C–H bond has a barrier (IM4d → TS2d) of 15.23 kcal mol^{-1}, which leads to the formation of the stable intermediate IM5d with a relative free energy of −33.96 kcal mol^{-1}. From the PES it has been observed that the formation of methanol is more favorable with an activation barrier (IM5d → TS3d) of 19.34 kcal mol^{-1} compared to the 2nd C–H bond activation with a barrier of (IM5d → TS3d′) 29.79 kcal mol^{-1}. The lower energy barrier and observed preference for methanol formation over secondary C–H activation can be explained by the substantial donation of lp(O) → σ*(Pd–C) in TS3d. Finally, the product methanol is desorbed from the system with a desorption free energy of 20.63 kcal mol^{-1}. We have also calculated the desorption of methanol in the presence of one additional water molecule; however, contrary to the previous cases, desorption energy rather increases in this case. In the triplet spin state, in both the orientations of Al atoms, it has been observed that the N–O dissociation barrier is very less compared to the rest of the cases.

Table 1 presents the activation barriers for all transition states associated with the partial oxidation of methane to methanol using the given catalysts. The chart indicates that, in most instances, the activation barrier for the N–O dissociation phase is elevated, suggesting that it may be the rate-determining step. However, the scenario is different in the case of triplet spin counterparts of Pd^{2+}@ZSM-5, where N–O dissociation has the lowest activation barriers. A similar trend is observed in the case of the triplet spin state of Pd^{2+}@ZSM-5 with the Al–O–Si–O–Si–O–Al linkage, where the N–O dissociation barrier is quite low. Pd@ZSM-5 exhibits an almost barrierless C–H activation step and CH_3–OH recombination step, rendering siliceous zeolites advantageous for the partial oxidation of methane. The reduced desorption energy of methanol from the system also inhibits its

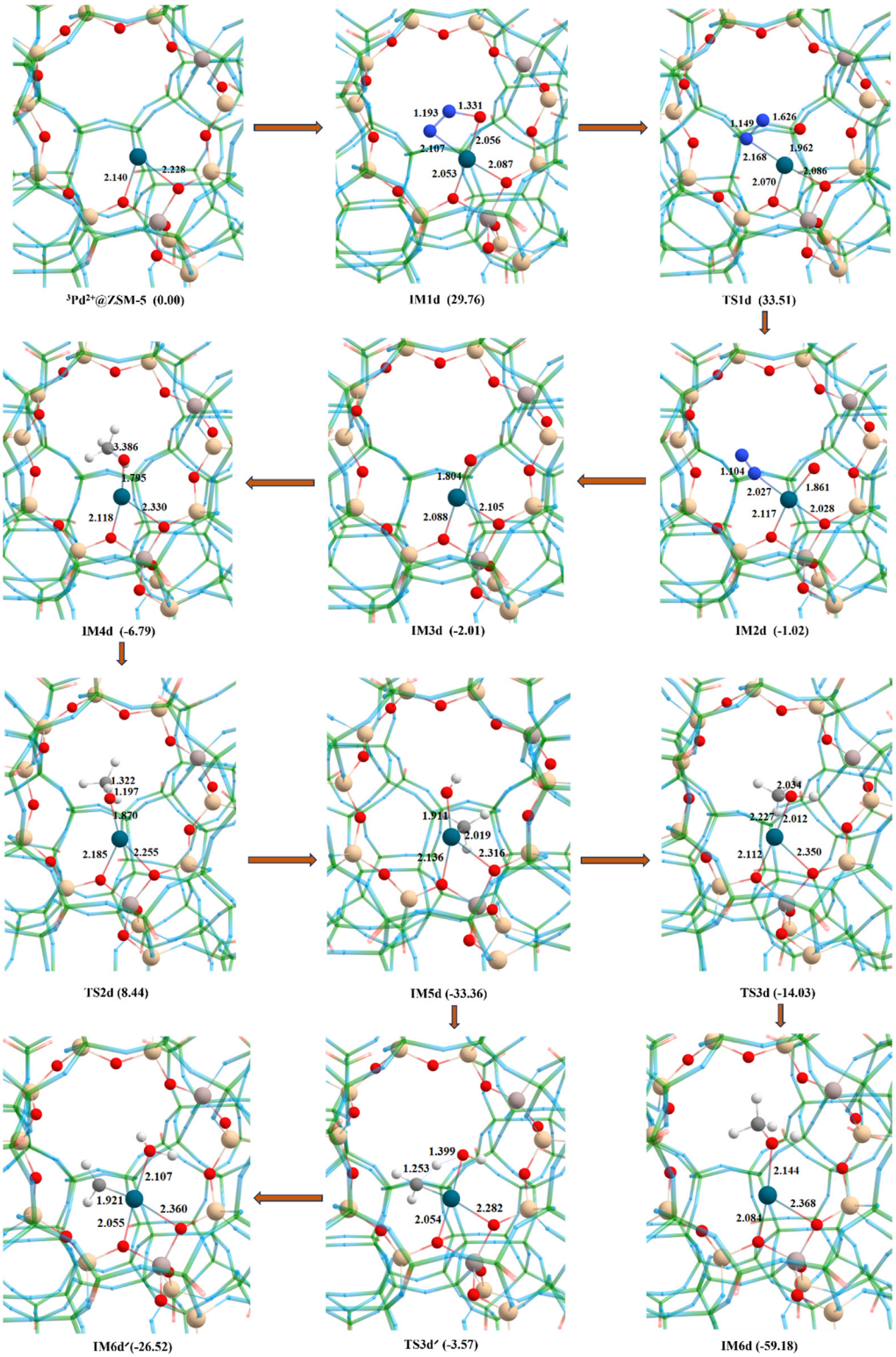

Fig. 8 Optimized diagrams involved in the partial oxidation of methane with Pd^{2+}@ZSM-5 with Al–O–Si–O–Si–Al–O linkage at a triplet spin state obtained from ONIOM calculations.

over-oxidation. Given that over-oxidation is a prevalent disadvantage of the oxidation reaction of methane, we have also assessed the activation of the methanol molecule generated in IM6 and it was found to be 30.77 kcal mol^{-1}. The computed disparity in barrier height indicates that the C–H activation of methane is favored over the activation of methanol.

In the case of Pd^{2+}@ZSM-5 (Al–O–Si–O–Al linkage), a spin crossover between triplet and singlet spin states is observed

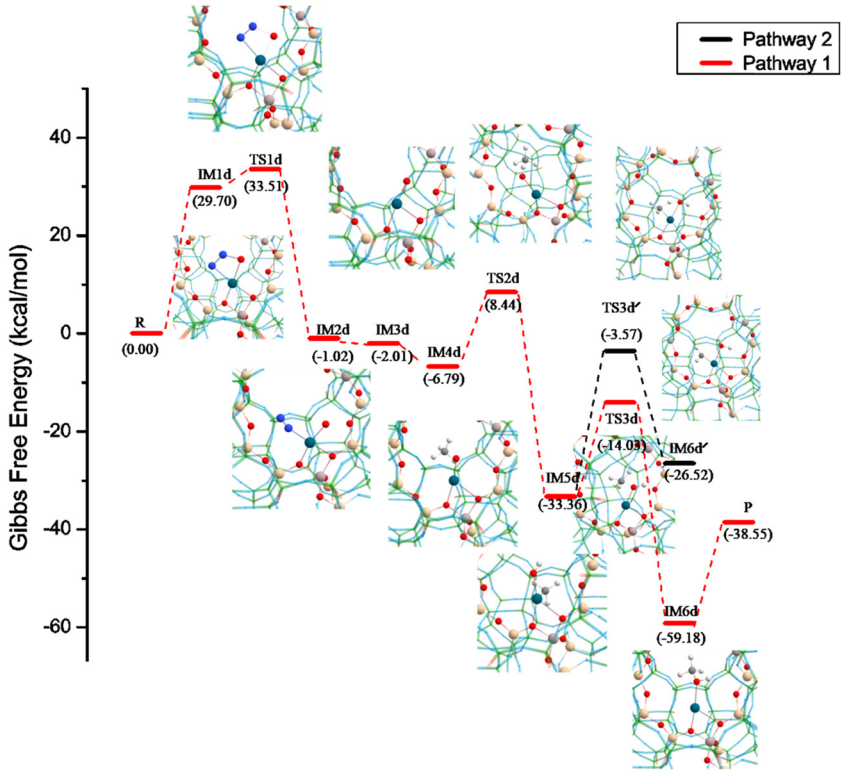

Fig. 9 PES of partial oxidation of methane to methanol *via* a triplet state on Pd^{2+}@ZSM-5 (Al–O–Si–O–Si–Al–O linkage).

during the reaction pathway due to their low-lying 1st excited state. However, after changing the position of the 2nd Al atom, the energy gap between singlet and triplet spin states increases and the triplet spin state becomes the ground spin state.

Kinetic study of the partial oxidation of methane to methanol

The rate coefficients of the partial oxidation of methane to methanol are calculated using the formula mentioned in Section 2.1 and the values are tabulated in Table 2.

The reaction involves three elementary steps during the pathway and one additional step to compare the last step of the reaction. From Table 2, it has been observed that the rate constant is the highest for the C–H activation of methane in all the cases, indicating their kinetic feasibility except in $^3Pd^{2+}$@ZSM-5. On the other hand, the rate determining step (RDS) in most of the cases is the N–O dissociation step except in $^3Pd^{2+}$@ZSM-5, where the CH_3–OH recombination step is the RDS. All the rate constants are found to be in the kinetically feasible range. The findings indicate that Pd@ZSM-5 systems demonstrate enhanced kinetic preference for the partial oxidation of methane to methanol.

Conclusion

In the quest for effective catalytic systems for methane oxidation, single-atom catalysts (SACs) have surfaced as very intriguing possibilities. Their remarkable reactivity, selectivity, and catalytic effectiveness arise from the existence of well-confined, low-coordinated metal centers, which are similar to enzyme active sites when integrated inside the microporous structures of zeolites. The present work based on the DFT-D3 based ONIOM method offers detailed molecular insights into the influence of the oxidation states of Pd (0, +1, and +2) and the surrounding zeolite environment for the selective partial oxidation of methane to methanol. The desired reaction pathway mainly consists of three elementary steps of N–O dissociation, C–H activation and CH_3–OH recombination steps. In the case of Pd(0) and Pd(I), the formation of the active site has the higher activation barrier and is also the rate determining step. Two-state reactivity was observed in the case of Pd^{2+}@ZSM-5 with the Al–O–Si–O–Al linkage, attributed to the presence of close lying singlet and triplet spin states. In the case of $^1Pd^{2+}$@ZSM-5, which has a closed shell configuration, the N–O dissociation step has a higher activation barrier, thus making it kinetically unfavorable. On the other hand, its triplet counterpart performs way better in N–O cleavage due to its favorable configuration. These findings suggest a spin state dependent pathway that mimics the enzyme like reactivity in the micro-porous zeolites.

A shift in the reactivity of the zeolites was found following the substitution of the Al atom in the MFI framework. The findings indicate how siliceous zeolites show better activity and selectivity compared to the Al-substituted ZSM-5 framework, highlighting the influence of local framework polarity and the overall reactivity. The presence of the water molecule effectively improves the methanol desorption in Al-substituted ZSM-5 by lowering desorption energy, whereas its influence is much weaker in the siliceous counterpart. These findings reveal that

Table 2 Values of the rate constant (in s^{-1}) for the reaction steps involved in the partial oxidation of methane to methanol

Reactions	Rate constant			
	k_1 (N–O dissociation)	k_2 (C–H activation)	k_3 (CH_3–OH recombination)	k'_3 (2nd C−H activation)
Pd@ZSM-5 + N_2O + CH_4 → Pd@ZSM-5 + CH_3OH	5.17×10^{-4}	6.0×10^{12}	3.79×10^{12}	1.93×10^{-2}
Pd^+@ZSM-5 + N_2O + CH_4 → Pd^+@ZSM-5 + CH_3OH	4.96×10^{-18}	2.16×10^{8}	1.74×10^{5}	1.29×10^{-4}
$^1Pd^{2+}$@ZSM-5 + N_2O + CH_4 → $^1Pd^{2+}$@ZSM-5 + CH_3OH (Al–O–Si–O–Al)	5.56×10^{-25}	7.96×10^{2}	1.90	3.18×10^{-22}
$^3Pd^{2+}$@ZSM-5 + N_2O + CH_4 → $^3Pd^{2+}$@ZSM-5 + CH_3OH (Al–O–Si–O–Al)	5.09×10^{9}	6.24×10^{7}	4.52×10^{-4}	3.96×10^{9}
$^3Pd^{2+}$@ZSM-5 + N_2O + CH_4 → $^3Pd^{2+}$@ZSM-5 + CH_3OH (Al–O–Si–O–Si–O–Al)	1.34×10^{10}	1.45×10^{2}	4.83×10^{-2}	5.04×10^{-18}

combined effects of the metal oxidation state, spin state and framework composition play a crucial role in determining the reactivity and selectivity of products, providing a rational foundation to develop more efficient SACs for methane oxidation. Our study deals with the mechanism of methane oxidation along with kinetics as well as easy desorption to prevent over oxidation of methanol.

The cluster based ONIOM approach employed in our study is good enough for capturing reactivity at the individual active site; however, it does not fully represent the dynamics and long-range impacts of the zeolite's framework. Therefore, future computational studies in this area may involve periodic DFT and molecular dynamics simulations to more accurately capture framework stability and entropic effects in the catalytic mechanism. This approach would provide a deeper and more realistic understanding of catalyst stability and reactivity under operating conditions, thereby bridging the gap between theoretical modeling and experimental observations.

Author contributions

PD and RCD conceptualized the study. PD carried out the DFT investigations supervised by RCD. All the other authors helped in preparing and writing the manuscript.

Conflicts of interest

The authors declare no conflicts of interest.

Data availability

The data supporting this article have been included as a part of the supplementary information (SI). Supplementary information is available. See DOI: https://doi.org/10.1039/d5cp02968f.

Acknowledgements

PD is thankful to DST Inspire (DST/INSPIRE Fellowship/2020/IF200086) for financial assistance. RCD is thankful to CSIR (01/3080/21/EMR-II). We acknowledge the Bioinformatics Resources and Applications Facility (BRAF) of C-DAC, Pune for providing access to their supercomputing facility to carry out the calculations.

References

1 A. Zhumadilova, S. Zhigitova and M. Turalina, The impact of greenhouse gases on climate change, *Sci. Horiz.*, 2023, **26**, 97–109.
2 M. Filonchyk, M. P. Peterson, L. Zhang, V. Hurynovich and Y. He, Greenhouse gases emissions and global climate change: examining the influence of CO_2, CH_4, and N_2O, *Sci. Total Environ.*, 2024, **935**, 173359.
3 D. S. Reay, P. Smith, T. R. Christensen, R. H. James and H. Clark, Methane and global environmental change, *Annu. Rev. Environ. Resour.*, 2018, **43**, 165–192.
4 P. Schwach, X. Pan and X. Bao, Direct conversion of methane to value-added chemicals over heterogeneous catalysts: challenges and prospects, *Chem. Rev.*, 2017, **117**, 8497–8520.
5 J. H. Lunsford, Catalytic conversion of methane to more useful chemicals and fuels: a challenge for the 21st century, *Catal. Today*, 2000, **63**, 165–174.
6 H. Singh, C. Li, P. Cheng, X. Wang and Q. Liu, A critical review of technologies, costs, and projects for production of carbon-neutral liquid e-fuels from hydrogen and captured CO_2, *Energy Adv.*, 2022, **1**, 580–605.
7 D. Zhang, R. Wang, Z. Zhang, H. Yan, X. Zhou, H. Zhao and C. Yang, Industrial ultra-low-carbon methanol synthesis routes: techno-economic analysis, life cycle environment assessment and multi-dimensional sustainability evaluation, *Green Chem.*, 2025, **27**, 1747–1762.
8 in *Methanol: the basic chemical and energy feedstock of the future*, ed. M. Bertau, H. Offermanns, L. Plass, F. Schmidt, and H. J. Wernicke, Springer, Heidelberg, 2014, vol. 1.
9 T. Klein, Methanol: a future-proof fuel, *Future Fuel Strategies*, 2020, 1–42.
10 N. J. Gunsalus, A. Koppaka, S. H. Park, S. M. Bischof, B. G. Hashiguchi and R. A. Periana, Homogeneous functionalization of methane, *Chem. Rev.*, 2017, **117**, 8521–8573.
11 A. A. Latimer, A. R. Kulkarni, H. Aljama, J. H. Montoya, J. S. Yoo, C. Tsai, F. A. Pederson, F. Studt and J. K. Nørskov, Understanding trends in C–H bond activation in heterogeneous catalysis, *Nat. Mater.*, 2017, **16**, 225–229.
12 M. Ravi, V. L. Sushkevich, A. J. Knorpp, M. A. Newton, D. Palagin, A. B. Pinar, M. Ranocchihari and J. A. van Bokhoven, Misconceptions and challenges in methane-to-methanol over transition-metal-exchanged zeolites, *Nat. Catal.*, 2019, **2**, 485–494.
13 R. K. Srivastava, P. K. Sarangi, L. Bhatia, A. K. Singh and K. P. Shadangi, Conversion of methane to methanol:

technologies and future challenges, *Biomass Convers Biorefin.*, 2022, **12**, 1851–1875.
14 W. Huang, S. Zhang, Y. Tang, Y. Li, L. Nguyen, Y. Li and F. Tao, Low-temperature transformation of methane to methanol on Pd1O4 single sites anchored on the internal surface of microporous silicate, *Angew. Chem., Int. Ed.*, 2016, **55**, 13441–13445; S. D. Senanayake, J. A. RodriguezandJ. and F. Weaver, Low temperature activation of methane on metal-oxides and complex interfaces: insights from surface science, *Acc. Chem. Res.*, 2020, **53**, 1488–1497.
15 R. Balasubramanian and A. C. Rosenzweig, Structural and mechanistic insights into methane oxidation by particulate methane monooxygenase, *Acc. Chem. Res.*, 2007, **40**, 573–580.
16 A. Prajapati, B. A. Collins, J. D. Goodpaster and M. R. Singh, Fundamental insight into electrochemical oxidation of methane towards methanol on transition metal oxides, *Proc. Natl. Acad. Sci. U. S. A.*, 2021, **118**, e2023233118.
17 Y. X. Zhao, Z. Y. Li, Y. Yang and S. G. He, Methane activation by gas phase atomic clusters, *Acc. Chem. Res.*, 2018, **51**, 2603–2610.
18 G. Fu, X. Xu and H. Wan, Mechanism of methane oxidation by transition metal oxides: a cluster model study, *Catal. Today*, 2006, **117**, 133–137.
19 W. Zhao, Y. Shi, Y. Jiang, X. Zhang, C. Long, P. An, Y. Zhu, S. Shao, Z. Yan, G. Li and Z. Tang, Fe–O clusters anchored on nodes of metal–organic frameworks for direct methane oxidation, *Angew. Chem.*, 2021, **133**, 5875–5879.
20 J. Baek, B. Rungtaweevoranit, X. Pei, M. Park, S. C. Fakra, Y. S. Liu, R. Matheu, S. A. Alshmimri, S. Alshehri, C. A. Trickett, G. A. Somorjai and O. M. Yaghi, Bioinspired metal–organic framework catalysts for selective methane oxidation to methanol, *J. Am. Chem. Soc.*, 2018, **140**, 18208–18216.
21 H. Y. Chen, J. Lu, J. M. Fedeykoand and A. Raj, Zeolite supported Pd catalysts for the complete oxidation of methane, A critical review, *Appl. Catal., A*, 2022, **633**, 118534.
22 M. H. Mahyuddin, Y. Shiota and K. Yoshizawa, Methane selective oxidation to methanol by metal-exchanged zeolites: a review of active sites and their reactivity, *Catal. Sci. Technol.*, 2019, **9**, 1744–1768.
23 X. F. Yang, A. Wang, B. Qiao, J. U. N. Li, J. Liu and T. Zhang, Single-atom catalysts: a new frontier in heterogeneous catalysis, *Acc. Chem. Res.*, 2013, **46**, 1740–1748.
24 R. Sharma, H. Poelman, G. B. Marin and V. V. Galvita, Approaches for selective oxidation of methane to methanol, *Catal*, 2020, **10**, 194.
25 H. Zhang, G. Liu, L. Shi and J. Ye, Single-atom catalysts: emerging multifunctional materials in heterogeneous catalysis, *Adv. Energy Mater.*, 2018, **8**, 1701343.
26 J. Z. Qiu, J. Hu, J. Lan, L. F. Wang, G. Fu, R. Xiao, B. Ge and J. Jiang, Pure siliceous zeolite-supported Ru single-atom active sites for ammonia synthesis, *Chem. Mater.*, 2019, **31**, 9413–9421.
27 S. Tomar, B. S. Bhadoria, H. Jeong, J. H. Choi, S. C. Lee and S. Bhattacharjee, Single-atom Pd catalyst on a CeO_2(111) surface for methane oxidation: activation barriers and reaction pathways, *J. Phys. Chem. C*, 2024, **128**, 8580–8589.
28 P. Kumar, T. A. Al-Attas, J. Hu and M. G. Kibria, Single atom catalysts for selective methane oxidation to oxygenates, *ACS Nano*, 2022, **16**, 8557–8618.
29 J. Liu, B. R. Bunes, L. Zang and C. Wang, Supported single-atom catalysts: synthesis, characterization, properties, and applications, *Environ. Chem. Lett.*, 2018, **16**, 477–505.
30 S. Tang, W. Li, J. Jin, X. Zhang, Z. Shen and Y. Gui, Lean methane catalytic combustion using Pd/ZSM-5 catalysts prepared by ammonia evaporation method, *Mol. Catal.*, 2025, **579**, 115092.
31 L. J. Arachchige, A. Dong, T. Wang, H. Li, X. L. Zhang, F. Wang, H. Su and C. Sun, Mechanistic insights into direct methane oxidation to methanol on single-atom transition-metal-modified graphyne, *ACS Appl. Nano Mater.*, 2021, **4**, 12006–12016.
32 J. H. Wen, D. Guo and G. C. Wang, Structure-sensitivity of direct oxidation methane to methanol over Rh_n/ZrO_{2-x} (1 0 1) (n = 1, 4, 10) surfaces: a DFT study, *Appl. Surf. Sci.*, 2021, **555**, 149690.
33 A. Airi, M. Signorile, F. Bonino, P. Quagliotto, S. Bordiga, J. A. Martens and V. Crocella, Insights on a hierarchical MFI zeolite: a combined spectroscopic and catalytic approach for exploring the multilevel porous system down to the active sites, *ACS Appl. Mater. Interfaces*, 2021, **13**, 49114–49127.
34 Z. Sun, Q. Shu, Q. Zhang, S. Li, G. Zhu, C. Wang, J. Zhang, H. Li and Z. Huang, A hydrothermal synthesis process of ZSM-5 zeolite for VOCs adsorption using desilication solution, *Separations*, 2024, **11**, 39.
35 M. Mancinelli, N. Precisvalle, M. Ardit, G. Beltrami, L. Gigli, E. Catizzone, M. Migliori, G. Giordano and A. Martucci, Thermal stability of templated ZSM-5 zeolites: an in situ synchrotron X-ray powder diffraction study, *Microporous Mesoporous Mater.*, 2023, **362**, 112777.
36 Á. Szécsényi, E. Khramenkova, I. Y. Chernyshov, G. Li, J. Gascon and E. A. Pidko, Breaking linear scaling relationships with secondary interactions in confined space: a case study of methane oxidation by Fe/ZSM-5 zeolite, *ACS Catal.*, 2019, **9**, 9276–9284.
37 D. Kiani, S. Sourav, Y. Tang, J. Baltrusaitis and I. E. Wachs, Methane activation by ZSM-5-supported transition metal centers, *Chem. Soc. Rev.*, 2021, **50**, 1251–1268.
38 Z. Zhang, P. Han, L. Li, X. Zhang, X. Cheng, J. Lin, S. Wan, H. Xiong, Y. Yang and S. Wang, Confinement-Enhanced Selective Oxidation of Lignin Derivatives to Formic Acid Over Fe-Cu/ZSM-5 Catalysts Under Mild Conditions, *ChemSusChem*, 2022, **15**, e202200218.
39 X. Tang, L. Wang, B. Yang, C. Fei, T. Yao, W. Liu, Y. Lou, Q. Dai, Y. Cai, X. M. Cao, W. Zhan, Y. Guo, X. Q. Gong and Y. Guo, Direct oxidation of methane to oxygenates on supported single Cu atom catalyst, *Appl. Catal., B*, 2021, **285**, 119827.
40 H. Wang, W. Xin, Q. Wang, X. Zheng, Z. Lu, R. Pei, P. He and X. Dong, Direct methane conversion with oxygen and

CO over hydrophobic dB-ZSM-5 supported Rh single-atom catalyst, *Catal. Commun.*, 2022, **162**, 106374.
41 R. J. Bunting, J. Thompson and P. Hu, The mechanism and ligand effects of single atom rhodium supported on ZSM-5 for the selective oxidation of methane to methanol, *Phys. Chem. Chem. Phys.*, 2020, **22**, 11686–11694.
42 H. Liu, J. Li, X. Liang, H. Ren, H. Yin, L. Wang, D. Yang, D. Wang and Y. Li, Encapsulation of Pd single-atom sites in zeolite for highly efficient semihydrogenation of alkynes, *J. Am. Chem. Soc.*, 2024, **146**, 24033–24041.
43 W. Kumsung, M. Chareonpanich, P. Kongkachuichay, S. Senkan and A. Seubsai, Single and bimetallic catalyst screenings of noble metals for methane combustion, *Catal. Commun.*, 2018, **110**, 83–87.
44 S. H. Oh, P. J. Mitchell and R. M. Siewert, Methane oxidation over alumina-supported noble metal catalysts with and without cerium additives, *J. Catal.*, 1991, **132**, 287–301.
45 J. Oh, A. Boucly, J. A. van Bokhoven, L. Artiglia and M. Cargnello, Palladium catalysts for methane oxidation: old materials, new challenges, *Acc. Chem. Res.*, 2023, **57**, 23–36.
46 K. Eguchi and H. Arai, Low temperature oxidation of methane over Pd-based catalysts—effect of support oxide on the combustion activity, *Appl. Catal., A*, 2001, **222**, 359–367.
47 J. Wang and G. C. Wang, Dynamic evolution of methane oxidation on Pd-based catalysts: a reactive force field molecular dynamics study, *J. Phys. Chem. C*, 2022, **126**, 14201–14210.
48 W. S. Epling and G. B. Hoflund, Catalytic oxidation of methane over ZrO_2-supported Pd catalysts, *J. Catal.*, 1999, **182**, 5–12.
49 X. Tang, M. Wang, B. Tang, Y. Zhao, W. Zhan, Y. Guo, L. Wang, S. Dai and Y. Guo, Synthesis of Heteroatom Pd–ZrO_x Species on Zeolite for Complete Methane Oxidation, *Ind. Eng. Chem. Res.*, 2023, **62**, 8244–8252.
50 J. Lei, R. Niu, S. Wang and J. Li, The Pd/Na-ZSM-5 catalysts with different Si/Al ratios on low concentration methane oxidation, *Solid State Sci.*, 2020, **101**, 106097.
51 L. Luo, S. Wang, Z. Wu, Z. Qin, M. Dong, J. Wang and W. Fan, Influence of the ZSM-5 support acidity on the catalytic performance of Pd/ZSM-5 in lean methane oxidation, *Chem. Res. Chin. Univ.*, 2022, **38**, 229–236.
52 A. W. Petrov, D. Ferri, F. Krumeich, M. Nachtegaal, J. A. van Bokhoven and O. Kröcher, Stable complete methane oxidation over palladium based zeolite catalysts, *Nat. Commun.*, 2018, **9**, 2545.
53 Q. Dai, Q. Zhu, Y. Lou and X. Wang, Role of Brønsted acid site during catalytic combustion of methane over PdO/ZSM-5: dominant or negligible?, *J. Catal.*, 2018, **357**, 29–40.
54 A. W. Petrov, D. Ferri, O. Krocherand and J. A. van Bokhoven, Design of stable palladium-based zeolite catalysts for complete methane oxidation by post synthesis zeolite modification, *ACS Catal.*, 2019, **9**, 2303–2312.
55 S. Impeng, P. Khongpracha, C. Warakulwit, B. Jansang, J. Sirijaraensre, M. Ehara and J. Limtrakul, Direct oxidation of methane to methanol on Fe–O modified Grapheme, *RSC Adv.*, 2014, **4**, 12572–12578.
56 S. Wang, C. Li, C. Liu and W. Zhuang, On the Heterogeneity of Iron-Oxo Species in Zeolites for the Oxidation of Methane to Methanol by Nitrous Oxide: A Theoretical Perspective, *ChemCatChem*, 2025, **17**, e202401416.
57 L. Baldinelli, P. Belanzoni and G. Bistoni, Mechanism of Nitrous Oxide Activation in C (sp^2)–O Bond Formation Reactions Catalyzed by Nickel Complexes, *J. Am. Chem. Soc.*, 2024, **146**, 6016–6024.
58 L. W. Chung, W. M. C. Sameera, R. Ramozzi, A. J. Page, M. Hatanaka, G. P. Petrova, T. V. Harris, X. Li, Z. Ke, F. Liu, H. B. Li, L. Ding and K. Morokuma, The ONIOM method and its applications, *Chem. Rev.*, 2015, **115**, 5678–5796.
59 V. Pelmenschikov and P. E. Siegbahn, Catalytic mechanism of matrix metalloproteinases: two-layered ONIOM study, *Inorg. Chem.*, 2002, **41**, 5659–5666.
60 T. Vreven, K. S. Byun, I. Komáromi, S. Dapprich, J. A. Montgomery Jr, K. Morokuma and M. J. Frisch, Combining quantum mechanics methods with molecular mechanics methods in ONIOM, *J. Chem. Theory Comput.*, 2006, **2**, 815–826.
61 K. Sillar and P. Burk, Hybrid quantum chemical and density functional theory (ONIOM) study of the acid sites in zeolite ZSM-5, *J. Phys. Chem. B*, 2004, **108**, 9893–9899.
62 G. Iuzzolino, F. Perrella, M. Valadan, A. Petrone, C. Altucci and N. Rega, Photophysics of a nucleic acid–protein cross-linking model strongly depends on solvation dynamics: an experimental and theoretical study, *Phys. Chem. Chem. Phys.*, 2024, **26**, 11755–11769.
63 K. M. Farhan and P. K. Sajith, Unveiling Zeolite Confinement Effects on N_2O Decomposition Reaction over $[Cu_2(\mu\text{-}O)]^{2+}$ Active Sites, *Ind. Eng. Chem. Res.*, 2025, **64**, 5257–5268.
64 C. R. A. Catlow, R. G. Bell, J. D. Gale and D. W. Lewis, Modelling of structure and reactivity in zeolites, *Stud. Surf. Sci. Catal.*, 1995, **97**, 87–100.
65 A. A. Kolganov, A. A. Gabrienko, S. A. Yashnik, E. A. Pidko and A. G. Stepanov, Nature of the surface intermediates formed from methane on Cu-ZSM-5 zeolite: a combined solid-state nuclear magnetic resonance and density functional theory study, *J. Phys. Chem. C*, 2020, **124**, 6242–6252.
66 S. A. Nastase, C. R. A. Catlow and A. J. Logsdail, QM/MM study of the stability of dimethyl ether in zeolites H-ZSM-5 and HY, *Phys. Chem. Chem. Phys.*, 2021, **23**, 2088–2096.
67 A. V. Larin, The Loewenstein rule: the increase in electron kinetic energy as the reason for instability of Al–O–Al linkage in aluminosilicate zeolites, *Phys. Chem. Miner.*, 2013, **40**, 771–780.
68 R. G. Bell, R. A. Jackson and C. R. A. Catlow, Löwenstein's rule in zeolite A: a computational study, *Zeolites*, 1992, **12**, 870–871.
69 M. Boronat, P. M. Viruela and A. Corma, Reaction intermediates in acid catalysis by zeolites: prediction of the relative tendency to form alkoxides or carbocations as a function of hydrocarbon nature and active site structure, *J. Am. Chem. Soc.*, 2004, **126**, 3300–3309.
70 S. Chiodo, N. Russo and E. Sicilia, LANL2DZ basis sets recontacted in the framework of density functional theory, *J. Chem. Phys.*, 2006, **125**, 104107.

71 V. Bertani, C. Cavallotti, M. Masi and S. Carrà, Density functional study of the interaction of palladium clusters with hydrogen and CH_x Species, *J. Phys. Chem. A*, 2000, **104**, 11390–11397.
72 S. Grimme, J. Antony, S. Ehrlich and H. Krieg, A consistent and accurate ab initio parametrization of density functional dispersion correction (DFT-D) for the 94 elements H-Pu, *J. Chem. Phys.*, 2010, **132**, 154104.
73 C. J. Casewit, K. S. Colwell and A. K. Rappe, Application of a universal force field to organic molecules, *J. Am. Chem. Soc.*, 1992, **114**, 10035–10046.
74 R. E. Patet, S. Caratzoulas and D. G. Vlachos, Adsorption in zeolites using mechanically embedded ONIOM clusters, *Phys. Chem. Chem. Phys.*, 2016, **18**, 26094–26106.
75 C. Raksakoon and J. Limtrakul, Adsorption of aromatic hydrocarbon onto H-ZSM-5 zeolite investigated by ONIOM study, *J. Mol. Struct.: THEOCHEM*, 2003, **631**, 147–156.
76 S. Namuangruk, P. Pantu and J. Limtrakul, Investigation of ethylene dimerization over faujasite zeolite by the ONIOM method, *ChemPhysChem*, 2005, **6**, 1333–1339.
77 M. S. Yordanlı, R. Escobar, J. Meza, D. Akgül, Y. Zhao, A. Uzun, F. A. Akin, V. Aviyante, A. C. Atesin and T. A. Ateşin, DFT Study of the Mechanism of Selective Hydrogenation of Acetylene by Rhodium Single-Atom Catalyst Supported on HY Zeolite, *ChemPhysChem*, 2025, **26**, e202400867.
78 Y. Sun, X. Mao and S. Pei, A two-layer ONIOM study of thiophene cracking catalyzed by proton-and cation-exchanged FAU zeolites, *J. Mol. Model.*, 2016, **22**, 51.
79 C. Gonzalez and H. B. Schlegel, Improved algorithms for reaction path following: higher-order implicit algorithms, *J. Chem. Phys.*, 1991, **95**, 5853–5860.
80 J. P. Foster and F. Weinhold, Natural hybrid orbitals, *J. Am. Chem. Soc.*, 1980, **102**, 7211–7218.
81 M. J. Frisch, G. W. Trucks, H. B. Schlegel, G. E. Scuseria, M. A. Robb, J. R. Cheeseman, G. Scalmani, V. Barone, G. A. Petersson and H. Nakatsuji, *et al.*, *Gaussian 16, Revision A.03*, Gaussian Inc., Wallingford CT, 2016.
82 K. J. Laidler and J. Keith, *Chemical kinetics*, McGraw-Hill, New York, 1965, vol. 2.
83 A. Delabie, C. Vinckier, M. Flock and K. Pierloot, Evaluating the activation barriers for transition metal N_2O reactions, *J. Phys. Chem. A*, 2001, **105**, 5479–5485.
84 W. B. Tolman, Binding and activation of N_2O at transition-metal centers: recent mechanistic insights, *Angew. Chem., Int. Ed.*, 2010, **49**, 1018–1024.
85 L. Meng, X. Zhu and E. J. Hensen, Stable Fe/ZSM-5 nanosheet zeolite catalysts for the oxidation of benzene to phenol, *ACS Catal.*, 2017, **7**, 2709–2719.
86 A. V. Kucherov and M. Shelef, An in situ ESR study of Pd/H-ZSM-5 interaction with different adsorbents, *Catal. Lett.*, 2001, **75**, 19–24.
87 L. S. Stokes, D. M. Murphy, R. D. Farley, C. C. Rowlands and S. Bailey, EPR investigation of Pd I species in palladium-exchanged ZSM-5 and beta zeolites, *Phys. Chem. Chem. Phys.*, 1999, **1**, 621–628.
88 T. Li, A. Beck, F. Krumeich, L. Artiglia, M. K. Ghosalya, M. Roger, D. Ferri, O. Kröcher, V. Sushkevich, O. V. Safonova and J. A. van Bokhoven, Stable palladium oxide clusters encapsulated in silicalite-1 for complete methane oxidation, *ACS Catal.*, 2021, **11**, 7371–7382.
89 X. Chen, X. Shi, P. Chen, B. Liu, M. Liu, L. Chen, D. Ye, X. Tu, W. Fan and J. Wu, Unlocking high-efficiency methane oxidation with bimetallic Pd–Ce catalysts under zeolite confinement, *ACS Environ. Au*, 2023, **3**, 223–232.
90 K. Okumura, J. Amano, N. Yasunobu and M. Niwa, X-ray absorption fine structure study of the formation of the highly dispersed PdO over ZSM-5 and the structural change of Pd induced by adsorption of NO, *J. Phys. Chem. B*, 2000, **104**, 1050–1057.
91 Y. Tang, Y. Li and F. F. Tao, Activation and catalytic transformation of methane under mild conditions, *Chem. Soc. Rev.*, 2022, **51**, 376–423.
92 H. Nakamoto and H. Takahashi, Hydrophobic natures of zeolite ZSM-5, *Zeolites*, 1982, **2**, 67–68.
93 J. Van der Mynsbrugge, M. Head-Gordon and A. T. Bell, Computational modeling predicts the stability of both Pd^+ and Pd^{2+} ion-exchanged into H-CHA, *J. Mater. Chem. A*, 2021, **9**, 2161–2174.
94 A. Akça, Conversion of methane to methanol on C-doped boron nitride: a DFT study, *Comput. Theor. Chem.*, 2021, **1202**, 113291.
95 B. E. Snyder, M. L. Bols, R. A. Schoonheydt, B. F. Sels and E. I. Solomon, Iron and copper active sites in zeolites and their correlation to metalloenzymes, *Chem. Rev.*, 2017, **118**, 2718–2768.
96 Y. Zhang, J. Yu, Y. H. Yeh, R. J. Gorte, S. Rangarajan and M. Mavrikakis, An adsorption study of CH4 on ZSM-5, MOR, and ZSM-12 zeolites, *J. Phys. Chem. C*, 2015, **119**, 28970–28978.
97 B. F. Gherman, B. D. Dunietz, D. A. Whittington, S. J. Lippard and R. A. Friesner, Activation of the C–H bond of methane by intermediate Q of methane monooxygenase: a theoretical study, *J. Am. Chem. Soc.*, 2001, **123**, 3836–3837.
98 E. Kurnaz, M. F. Fellah and I. Onal, A density functional theory study of C–H bond activation of methane on a bridge site of M–O–M-ZSM-5 Clusters (M = Au, Ag, Fe and Cu), *Microporous Mesoporous Mater.*, 2011, **138**, 68–74.
99 X. Wang, A. Shishkin, F. Hemmingsson, M. Skoglundh, F. J. Martinez-Casado, L. Bock, A. Idström, L. Nordstierna, H. Härelend and P. A. Carlsson, Methane adsorption and methanol desorption of copper modified boron silicate, *RSC Adv.*, 2018, **8**, 36369–36374.
100 Z. Feng, X. Liu, Y. Wang and C. Meng, Recent advances on gallium-modified ZSM-5 for conversion of light hydrocarbons, *Molecules*, 2021, **26**, 2234.
101 D. Schröder, S. Shaik and H. Schwarz, Two-state reactivity as a new concept in organometallic chemistry, *Acc. Chem. Res.*, 2000, **33**, 139–145.
102 P. He and S. F. Zhu, Spin crossover and its application in organometallic catalysis: concepts and recent progress, *Chem. – Eur. J.*, 2024, **30**, e202403437.